



48 Correspondence:

49 [kmoberg@emory.edu](mailto:kmoberg@emory.edu) and [acorbe2@emory.edu](mailto:acorbe2@emory.edu)

50  
51 Running title: Nab2 interacts with PCP to pattern axons and dendrites

52  
53 Keywords: Nab2, RNA binding protein, planar cell polarity, mushroom body, axon, ddaC neuron,  
54 dendrite, intellectual disability

55  
56

57 **Abstract**

58 RNA binding proteins support neurodevelopment by modulating numerous steps in post-transcriptional  
59 regulation, including splicing, export, translation, and turnover of mRNAs that can traffic into axons and  
60 dendrites. One such RBP is ZC3H14, which is lost in an inherited intellectual disability. The *Drosophila*  
61 *melanogaster* ZC3H14 ortholog, Nab2, localizes to neuronal nuclei and cytoplasmic ribonucleoprotein  
62 granules, and is required for olfactory memory and proper axon projection into brain mushroom bodies.  
63 Nab2 can act as a translational repressor in conjunction with the Fragile-X mental retardation protein  
64 homolog Fmr1 and shares target RNAs with the Fmr1-interacting RBP Ataxin-2. However, neuronal  
65 signaling pathways regulated by Nab2 and their potential roles outside of mushroom body axons remain  
66 undefined. Here, we demonstrate that Nab2 restricts branching and projection of larval sensory dendrites  
67 via the planar cell polarity pathway, and that this link may provide a conserved mechanism through  
68 which Nab2/ZC3H14 modulates projection of both axons and dendrites. Planar cell polarity proteins are  
69 enriched in a Nab2-regulated brain proteomic dataset. Complementary genetic data indicate that Nab2  
70 guides dendrite and axon growth through the planar-cell-polarity pathway. Analysis of the core planar  
71 cell polarity protein Vang, which is depleted in the *Nab2* mutant whole-brain proteome, uncovers  
72 selective and dramatic loss of Vang within axon/dendrite-enriched brain neuropil relative to brain  
73 regions containing cell bodies. Collectively, these data demonstrate that Nab2 regulates dendritic arbors  
74 and axon projection by a planar-cell-polarity-linked mechanism and identify Nab2 as required for  
75 accumulation of the core planar cell polarity factor Vang in distal neuronal projections.

76

77

## 78 **Introduction**

79 While many key developmental events are triggered by extracellular factors that signal through  
80 cytoplasmic cascades to alter nuclear gene transcription, other key events are triggered by shifts in  
81 posttranscriptional processing or localization of mRNAs that guide cell fates and differentiation.  
82 Importantly, the fidelity of these mRNA-based developmental mechanisms relies on RNA binding  
83 proteins (RBPs) that associate with nascent RNAs and regulate splicing, export, stability, localization,  
84 and translation (SCHIEWECK *et al.* 2021). These key regulatory mechanisms are particularly evident in  
85 the developing nervous system, where mutations in genes encoding RBPs are often linked to human  
86 diseases. Examples of this linkage include Fragile X mental retardation protein (FMRP) (GROSS *et al.*  
87 2012), the survival of motor neuron protein (SMN) (EDENS *et al.* 2015), and the TAR DNA binding  
88 protein 43 (TDP-43) (AGRAWAL *et al.* 2019; GEBAUER *et al.* 2021). Sensitivity of the central and  
89 peripheral nervous systems to loss of RBPs has been attributed to the importance of post-transcriptional  
90 mechanisms, such as local translation of mRNAs and brain-specific extension of 3'UTRs (MATTIOLI *et*  
91 *al.* 2017; THELEN AND KYE 2019; ENGEL *et al.* 2020) that enable fine-tuned spatiotemporal control of  
92 neuronal gene expression. This spatiotemporal control of mRNA processing and translation plays an  
93 important role in forming complex dendritic architectures and the uniquely polarized morphology of  
94 neurons (LEE *et al.* 2003). Accordingly, neurological diseases caused by mutations in genes encoding  
95 RBPs often include defects in axonal or dendritic morphology (JUNG *et al.* 2012; HORNBERG AND HOLT  
96 2013; HOLT *et al.* 2019), and in some cases, these axonal and dendritic defects can be traced to defective  
97 post-transcriptional control of one or a few mRNAs normally bound by the corresponding RBP.

98 The human *ZC3H14* gene encodes a ubiquitously expressed zinc-finger, polyadenosine RBP (ZnF  
99 CysCysCysHis #14) that is lost in an inherited form of intellectual disability (PAK *et al.* 2011). Studies  
100 in multiple model organisms have begun to define functions for *ZC3H14* in guiding neuronal  
101 morphogenesis. Analysis of the sole *Drosophila* *ZC3H14* homolog, Nab2, detects cell-autonomous  
102 requirements in Kenyon cells (KCs) for olfactory memory as well as axonal branching and projection

103 into the brain mushroom bodies (MBs) (KELLY *et al.* 2016; BIENKOWSKI *et al.* 2017), twin neuropil  
104 structures that are the center for associative olfactory learning in insects (THUM AND GERBER 2019).  
105 Significantly, transgenic expression of human ZC3H14 only in fly neurons is sufficient to rescue a  
106 variety of *Nab2* null phenotypes (PAK *et al.* 2011; KELLY *et al.* 2014; KELLY *et al.* 2016), supporting a  
107 model in which Nab2 and ZC3H14 share critical molecular roles and mRNA targets. The *Zc3h14* gene  
108 is not essential in mice but its loss results in defects in working memory (RHA *et al.* 2017) and dendritic  
109 spine morphology (JONES *et al.* 2021). An accompanying proteomic analysis of *Zc3h14* knockout  
110 hippocampi identified several proteins involved in synaptic development and function that change in  
111 abundance upon ZC3H14 loss (RHA *et al.* 2017), and which are thus candidates to contribute to *Zc3h14*  
112 mutant phenotypes. Intriguingly, the homologs of some of these ZC3H14-regulated proteins in the  
113 mouse hippocampus are also sensitive to Nab2 loss in the developing *Drosophila* pupal brain (CORGIAT  
114 *et al.* 2021), suggesting conserved links between Nab2 and ZC3H14 and neurodevelopmental pathways.

115 A variety of intercellular signaling mechanisms play required roles in sensing extracellular cues  
116 that guide the complex axonal and dendritic structures that characterize specific areas of the central and  
117 peripheral nervous system (CNS and PNS). These cascades can respond to long-range directional cues,  
118 such as Netrin signaling, or to short-range directional cues from the Slit-Robo, Abl-Ena, and  
119 Semaphorin pathways (PURAM AND BONNI 2013; STOECKLI 2018). One pathway with an emerging role  
120 in both axonal and dendritic development is the planar cell polarity (PCP)-noncanonical Wnt pathway  
121 (ZOU 2004; ANDRE *et al.* 2012; ZOU 2012; GOMBOS *et al.* 2015; MISRA *et al.* 2016). PCP signals are  
122 based on asymmetric distribution of two apically localized transmembrane complexes, which in  
123 *Drosophila* correspond to the Stan-Vang-Pk complex (Starry Night aka Flamingo-Van Gogh-Prickle)  
124 and the Stan-Fz-Dsh-Dgo complex (Frizzled-Disheveled-Diego); these complexes are intracellularly  
125 antagonistic but intercellularly attractive, leading to apical polarization across an epithelial plane  
126 (TAYLOR *et al.* 1998; BOUTROS AND MLODZIK 1999; VLADAR *et al.* 2009; GOODRICH AND STRUTT 2011;

127 ADLER 2012; PENG AND AXELROD 2012; ADLER AND WALLINGFORD 2017; MLODZIK 2020). Core PCP  
128 components signal to downstream effector molecules that exert localized effects on the F-actin  
129 cytoskeleton (COURBARD *et al.* 2009; ADLER 2012; SOLDANO *et al.* 2013; FAGAN *et al.* 2014; GOMBOS  
130 *et al.* 2015), which in turn guides epithelial traits like proximal-distal wing hair orientation in  
131 *Drosophila* and sensory hair cell polarity in the mouse cochlea (JONES AND CHEN 2007; QIAN *et al.*  
132 2007; SIMONS AND MLODZIK 2008; CHACON-HESZELE AND CHEN 2009; RIDA AND CHEN 2009;  
133 ALPATOV *et al.* 2014). One such factor is encoded by the  $\beta$  amyloid protein precursor-like (*Appl*) gene  
134 and modulates the PCP pathway during axonal and dendritic outgrowth (SOLDANO *et al.* 2013; LIU *et al.*  
135 2021). Importantly, PCP is required for axon guidance in specific groups of neurons in *Drosophila*, *C.*  
136 *elegans*, mice, and chick, and for dendritic branching of mouse cortical and hippocampal neurons, and  
137 *Drosophila* body wall sensory neurons (HINDGES *et al.* 2002; McLAUGHLIN AND O'LEARY 2005;  
138 SCHMITT *et al.* 2006; SHAFER *et al.* 2011; CANG AND FELDHEIM 2013; YOSHIOKA *et al.* 2013;  
139 HAGIWARA *et al.* 2014; YASUMURA *et al.* 2021). For example, loss of the murine *Vang* homolog *Vangl2*  
140 leads to defects in axon guidance of spinal cord commissural axons (SHAFER *et al.* 2011), and *dsh*  
141 mutants in *C. elegans* cause neuronal projection and morphology defects (ZHENG *et al.* 2015). In  
142 *Drosophila*, loss of the core PCP components *stan*, *Vang*, *pk*, *fz*, or *dsh* individually disrupt  $\alpha$  and  $\beta$   
143 axon projection into the MBs (SHIMIZU *et al.* 2011; NG 2012). Intriguingly, loss of *stan* or its LIM-  
144 domain adaptor *espinas* (*esn*) also disrupts dendritic self-avoidance among the class IV dendritic  
145 arborization (da) neurons (MATSUBARA *et al.* 2011), demonstrating a requirement for PCP factors in  
146 both axon and dendrite morphogenesis within sets of neurons in the central (CNS) and peripheral (PNS)  
147 nervous systems.

148 Integrating data from two of our recent studies provides evidence for pathways through which the  
149 Nab2 RBP could guide axonal and dendritic projections. These analyses, one a genetic modifier screen  
150 based on a *GMR-Nab2* rough eye phenotype (LEE *et al.* 2020) and the other a proteomic analysis of

151 *Nab2* null pupal brains (CORGIAT *et al.* 2021), each suggest a link between *Nab2* and the PCP pathway.  
152 The *GMR-Nab2* modifier screen identified alleles of PCP components, both core components and  
153 downstream effectors (e.g., *Vang*, *dsh*, *fz*, *stan*, *pk*, *Appl*, and the formin *DAAM*), as dominant modifiers  
154 of *Nab2* overexpression phenotypes in the retinal field (LEE *et al.* 2020). In parallel, gene ontology (GO)  
155 analysis of proteomic changes in *Nab2* null brains detected enrichment for dendrite guidance and  
156 axodendritic transport GO terms among affected proteins (CORGIAT *et al.* 2021), which include the core  
157 PCP factor *Vang* and the PCP accessory factor A-kinase anchor protein 200 (Akap200). Significantly,  
158 *Drosophila* *Vang* and its murine homolog *Vangl2* are one of six pairs of homologs whose levels change  
159 significantly in *Nab2* null fly brains and *Zc3h14* knockout mouse hippocampi (RHA *et al.* 2017;  
160 CORGIAT *et al.* 2021), suggesting a conserved relationship between *Nab2/ZC3H14* and the PCP pathway  
161 in the metazoan central nervous system (CNS).

162       Considering observations outlined above, we have investigated interactions between *Nab2* and  
163 PCP factors in two neuronal contexts - CNS axons of the *Drosophila* pupal MB  $\alpha$ - and  $\beta$ -lobes, and in  
164 larval dendrites of class IV dorsal dendritic arbor C (ddaC) neurons - which provide complementary  
165 settings to analyze the *Nab2*-PCP link in axonal and dendritic compartments. We detect enrichment for  
166 PCP factors among brain-enriched proteins affected by *Nab2* loss and a pattern of genetic interactions  
167 between *Nab2* and multiple PCP alleles in both MB axons and ddaC dendrites that are consistent with  
168 *Nab2* regulating axon and dendrite outgrowth by a common PCP-linked mechanism. However,  
169 differences in how individual PCP alleles modify axonal vs dendritic *Nab2* mutant phenotypes suggest  
170 that the *Nab2*-PCP relationship may vary between neuronal subtypes (i.e., pupal Kenyon cells vs. larval  
171 ddaC neurons). Cell type-specific RNAi indicates that *Nab2* acts cell autonomously to guide PCP-  
172 dependent axon and dendrite growth, implying a potentially direct link between *Nab2* and one or more  
173 PCP components within Kenyon cells and ddaC neurons. Based on the drop in *Vang* levels detected by  
174 proteomic analysis of *Nab2* null brains (CORGIAT *et al.* 2021), we analyze the levels and distribution of a

Corgiat et al.

175 fluorescently tagged Vang protein in adult fly brains. Consistent with prior bulk proteomic data, overall  
176 Vang-GFP fluorescence is reduced in *Nab2* null brains compared to control; significantly, this drop is  
177 accompanied by an unexpected and selective loss of Vang protein in neuropil regions enriched in axons  
178 compared to regions enriched in cell bodies. Collectively, these data demonstrate that Nab2 is required  
179 to regulate axonal and dendritic growth through a PCP-linked mechanism and identify the Nab2 RBP as  
180 required for the accumulation of Vang protein into distal axonal compartments.

181

182



183 **Materials and Methods:**

184 ***Drosophila* genetics.** All crosses were maintained in humidified incubators at 25°C with 12hr light-dark  
185 cycles unless otherwise noted. The *Nab2<sup>ex3</sup>* loss of function mutant has been described previously (PAK  
186 *et al.* 2011). Alleles and transgenes: *Nab2<sup>EP3716</sup>* (referred to as “*Nab2 oe*”; Bloomington (BL) #17159),  
187 *UAS-Nab2<sup>RNAi</sup>* (Vienna *Drosophila* Research Center (VDRC), #27487), *UAS-fz2<sup>RNAi</sup>* (BL #27568), *appl<sup>d</sup>*  
188 (BL #43632), *dsh<sup>l</sup>* (BL #5298), *Vang<sup>stbm-6</sup>* (BL #6918), *pk<sup>pk-sple-13</sup>* (BL #41790), *Vang<sup>EGFP.C</sup>* (‘*Vang-*  
189 *eGFP*’) (gift of D. Strutt), *ppk-Gal4;UAS-mCD8::GFP* (gift of D. Cox), and *w<sup>1118</sup>* (‘control’).

190 ***Drosophila* brain dissection, immunohistochemistry, visualization, and statistical analysis.** Brain  
191 dissections were performed essentially as previously described (KELLY *et al.* 2016). Briefly, 48-72 hours  
192 after puparium formation (APF) brains were dissected in PBS (1xPBS) at 4°C, fixed in 4%  
193 paraformaldehyde at RT, washed 3x in PBS, and then permeabilized in 0.3% PBS-T (1xPBS, 0.3%  
194 TritonX-100). Following blocking for 1hr (0.1% PBS-T, 5% normal goat serum), brains were stained  
195 overnight in block+primary antibodies. After 5x washes in PBS-T (1xPBS, 0.3% TritonX-100), brains  
196 were incubated in block for 1hr, moved into block+secondary antibody for 3hrs, then washed 5x in PBS-  
197 T and mounted in Vectashield (Vector Labs). Antibodies used: anti-FasII 1D4 (Developmental Studies  
198 Hybridoma Bank) at 1:50 dilution, anti-GFP polyclonal (ThermoFisher Catalog# A-11122) at a 1:200  
199 dilution, and anti-nc82 (Developmental Studies Hybridoma Bank) at 1:50 dilution. Whole brain images  
200 were captured on a Nikon AR1 HD25 confocal microscope using NIS-Elements C Imaging software  
201 v5.20.01, and maximum intensity projections were generated in ImageJ Fiji. Mushroom body  
202 morphological defects were called as  $\alpha$ -lobe thinning or missing and  $\beta$ -lobe fusion or missing for  
203 *control*, *Nab2<sup>ex3</sup>*, and control and experimental PCP alleles (e.g., *Vang<sup>stbm-6/+</sup>*, *appl<sup>d/+</sup>*, and *dsh<sup>l/+</sup>*  
204 paired with *control* or *Nab2<sup>ex3</sup>*). Statistical analyses for MB phenotypes and plotting performed using  
205 GraphPad Prism8™. Significance determined using student’s t-test or ANOVA as indicated in figure  
206 legends. Error bars representing standard deviation. Significance scores indicated are \* $p \leq 0.05$ ,

207 \*\* $p \leq 0.01$ , and \*\*\* $p \leq 0.001$ . Vang-eGFP fluorescence intensity was quantified using two isolated regions  
208 of interest (ROI). One ROI located at right hemisphere dorsal cortical surface above the  $\alpha$ -lobe (referred  
209 to as cortical surface ROI) and a second ROI located at left hemisphere central complex neuropil  
210 approximately near the  $\beta$ -lobe and ellipsoid body (referred to as central neuropil ROI). The fluorescence  
211 intensity of each ROI was measured in *control* (n=9) and *Nab2<sup>ex3</sup>* (n=9) brains. Significance determined  
212 using student's t-test; significances scores indicated by \* =  $p < 0.05$ .

213 ***Drosophila* neuron live imaging confocal microscopy, neuronal reconstruction, data analyses, and**  
214 **statistical analysis.** Live imaging of class IV dorsal dendritic arbor C (ddaC) neurons was performed  
215 essentially as described as described in (IYER *et al.* 2013; CLARK *et al.* 2018). Briefly, 3rd instar *ppk-*  
216 *Gal4,mCD8::GFP* labelled larvae were mounted in 1:5 (v/v) diethyl ether:halocarbon oil under an  
217 imaging bridge of two 22x22mm glass coverslips topped with a 22x50mm glass coverslip. ddaC images  
218 were captured on an Olympus FV 1000 BX61WI upright microscope using Olympus Fluoview software  
219 v4.2. Maximum intensity projections were generated with ImageJ Fiji. Neuronal reconstruction was  
220 performed with the TREES toolbox (THEISEN *et al.* 1994). MathWorks Matlab R2010a v7.10.0.499  
221 (Natick, MA) was used to process 2D stacks with local brightness thresholding, skeletonization, and  
222 sparsening to leave carrier points (CUNTZ *et al.* 2010). Dendritic roots were defined at the soma and used  
223 to create synthetic dendritic arbors. Reconstruction parameters were equivalent across neurons. Various  
224 morphological metrics were obtained using the TREES toolbox including: Sholl analysis, total cable  
225 length, maximum path length, number of branch points, mean path/Euclidean distance, maximum  
226 branch order, mean branch order, mean branch angle, mean path length, mean branch order, field  
227 height/width, center of mass x, and center of mass y. These metrics were extracted in batch processing  
228 using in-house custom scripts and exported into RStudio v1.1.453 (Vienna, Austria), where  
229 quantification was visualized using other in-house custom scripts. Statistical analyses for ddaC  
230 phenotypes and plotting were performed using RStudio and Matlab. Balloon plots showing phenotypic

231 data generated using either ddaC measurements generated in Matlab or MB defect counts. Balloon plots  
232 generated using RStudio v1.1.453 ggpubr v0.2 (ALBOUKADEL 2018; R-TEAM 2018).

### 233 **Global proteomics**

234 MS/MS-LC data was previously described in (CORGIAT *et al.* 2021). Briefly, ten biological replicates of  
235 24 hr apf control ( $w^{1118}$ ) or  $Nab2^{ex3}$  pupal brains (60 brains per replicate) were lysed in urea buffer (8 M  
236 urea, 100 mM NaHPO<sub>4</sub>, pH 8.5) with HALT protease and phosphatase inhibitor (Pierce/Thermo  
237 Scientific) and processed at the Emory Proteomics Core. Separate samples were prepared for male and  
238 female brains. Label-free quantification analysis was adapted from a previously published procedure  
239 (SEYFRIED *et al.* 2017). Data was analyzed using MaxQuant v1.5.2.8 with Thermo Foundation 2.0 for  
240 RAW file reading capability. Spectra were searched using the search engine Andromeda and integrated  
241 into MaxQuant against the *Drosophila melanogaster* Uniprot database (43,836 target sequences).  
242 Analyses presented here used RStudio v1.1.453 (R-TEAM 2018), custom in-house scripts, and the  
243 following packages: ggpubr v0.2 (ALBOUKADEL 2018), cluster v2.1.0 (MAECHLER *et al.* 2016 ), and  
244 GOplot v1.0.2 (WALTER *et al.* 2015), to examine ‘planar cell polarity’ annotated proteins. Gene  
245 ontology analyses were performed using FlyEnrichr (FlyEnrichr:amp.pharm.mssm.edu/FlyEnrichr/)  
246 (CHEN *et al.* 2013; KULESHOV *et al.* 2016; KULESHOV *et al.* 2019), a *Drosophila* specific gene ontology  
247 enrichment analysis package.

### 248 **Mouse strain, animal care, and histologic analysis of inner ear tissues**

249 The  $Zc3h14^{\Delta ex13/\Delta ex13}$  mouse line has been (referred to as  $Zc3h14^{\Delta 13/\Delta 13}$  or  $\Delta 13/\Delta 13$ ) described previously  
250 (RHA *et al.* 2017). Generations F4-F8 of  $Zc3h14^{\Delta ex13/\Delta ex13}$  backcrosses were used with  $Zc3h14^{+/+}$   
251 controls. All procedures involving mice were done in accordance with HHU guidelines and approved by  
252 the Emory University Institutional Animal Care and Use Committee. Cochlea dissection, sectioning, and  
253 immunostaining from E14.5 animals has been described previously in (RADDE-GALLWITZ *et al.* 2004).  
254 Whole-mounts of organs of Corti were stained with FITC-conjugated phalloidin to label the stereocilia

Corgiat et al.

255 as in (WANG *et al.* 2005; QIAN *et al.* 2007) and samples were analyzed and imaged using a Zeiss  
256 LSM510. Cochlear morphological defects were called as extra based on a three OHC layers and one  
257 ICH layer separated by pillar cell region. Significance determined using student's t-test; significance  
258 scores indicated by \* $p < 0.05$

259

260

261 **Results**

262 **Nab2 loss alters levels of planar cell polarity pathway proteins in the *Drosophila* brain.**

263 Our recent study comparing proteomic changes in *Drosophila* pupal brains lacking Nab2 identified  
264 *planar cell polarity* gene ontology (GO) terms as one category of significantly altered factors (CORGIAT  
265 *et al.* 2021) (**Fig. 1A**). A deeper analysis of this protein dataset detects enrichment of five PCP-related  
266 GO terms (*establishment of planar polarity, establishment of epithelial cell planar polarity,*  
267 *establishment of body hair or bristle planar polarity, protein localization involved in planar polarity,*  
268 *regulation of establishment of planar polarity*) (**Fig. 1B**) extracted from 17 PCP-annotated proteins,  
269 including the core PCP component Van Gogh (Vang), and five putative PCP effectors: the Tumbleweed  
270 GTPase activating protein (GAP) (SOTILLOS AND CAMPUZANO 2000; JONES *et al.* 2010), the neuron-  
271 specific PCP modulator Appl (SINGH AND MLODZIK 2012; SOLDANO *et al.* 2013; LIU *et al.* 2021), the  
272 anchoring protein Akap200 (JACKSON AND BERG 2002; WEBER *et al.* 2012; BALA TANNAN *et al.* 2018),  
273 the endocytic regulator X11L $\beta$  (GROSS *et al.* 2013), and the muscle LIM-domain protein at 84B  
274 (Mlp84B) (WEBER *et al.* 2012). Together these factors represent 6.4% of the total differentially  
275 expressed proteins in *Nab2<sup>ex3</sup>* pupal brains relative to control (346 proteins in total) (see CORGIAT *et al.*  
276 2021) (**Table S1**). The Vang protein (decreased 5-fold in *Nab2<sup>ex3</sup>* vs control) and Appl protein  
277 (increased 1.5-fold in *Nab2<sup>ex3</sup>* vs control) are particularly notable because alleles of these genes  
278 dominantly modify phenotypes produced by *GMR-Gal4* driven Nab2 overexpression in the developing  
279 retinal field (LEE *et al.* 2020).

280 **Planar cell polarity components dominantly modify Nab2 axonal phenotypes.**

281 To pursue the Nab2-PCP link in the developing CNS, we tested whether axon projection defects in MBs  
282 homozygous for the *Nab2<sup>ex3</sup>* null allele (PAK *et al.* 2011) are sensitive to subtle modulation of PCP  
283 pathway activity using single copies of loss-of-function alleles of PCP components. Our previous work  
284 established genetic interactions between Nab2 and an array of PCP/Wnt alleles in the adult *Drosophila*

285 eye (LEE *et al.* 2020). Here, we focused on three of these factors: the core PCP/Wnt factor Vang, which  
286 proteomic data indicate is reduced 5-fold in *Nab2<sup>ex3</sup>* brains (CORGIAT *et al.* 2021), the accessory factor  
287 Appl (Amyloid precursor protein-like), which is a proposed PCP/Wnt co-receptor and has established  
288 links to neurological disease (SINGH AND MLODZIK 2012; SOLDANO *et al.* 2013; LIU *et al.* 2021), and the  
289 PCP/Wnt cytoplasmic adaptor Dsh, which also genetically interacts with *Nab2* in the wing to control  
290 hair polarity (LEE *et al.* 2020). As has been observed in *Nab2<sup>ex3</sup>* adult brains (KELLY *et al.* 2016;  
291 BIENKOWSKI *et al.* 2017), *Nab2<sup>ex3</sup>* mutant pupal brain at 48-72h APF (after puparium formation) display  
292 highly penetrant defects in structure of the  $\alpha$ -lobes (85% thinned or missing) and  $\beta$ -lobes (88% fused or  
293 missing) as detected by anti-Fas2 staining (**Fig. 2A-D,Q,R**). Both the *Vang<sup>stbm6</sup>* and *Appl<sup>d</sup>* loss-of-  
294 function alleles have no effect on MB structure in an otherwise wildtype background but suppress the  
295 frequency of *Nab2<sup>ex3</sup>*  $\alpha$ -lobe defects from 85% to 49% in a *Vang<sup>stbm6</sup>/+* heterozygous background and to  
296 62% in a *Appl<sup>d</sup>/+* heterozygous background; the frequency of *Nab2<sup>ex3</sup>*  $\beta$ -lobe defects drops from 88% to  
297 33% in *Vang<sup>stbm6</sup>/+* heterozygous background and to 35% in *Appl<sup>d</sup>/+* heterozygous background (**Fig.**  
298 **2E-F,I-J,M-N**). The PCP-specific allele *dsh<sup>l</sup>* (THEISEN *et al.* 1994; GOMBOS *et al.* 2015) lowers *Nab2<sup>ex3</sup>*  
299  $\alpha$ -lobe defects from 85% to 63% but has no effect on the frequency or severity of *Nab2<sup>ex3</sup>*  $\beta$ -lobe defects  
300 (**Fig. 2Q,R**) (**Fig. S1**). Intriguingly, animals with single copies of *Vang<sup>stbm6</sup>*, *Appl<sup>d</sup>*, and *dsh<sup>l</sup>* in the  
301 *Nab2<sup>ex3</sup>* homozygous background also develop a MB phenotype not observed in any single mutant: a  
302 bulbous, Fas2-positive lobe at the point at which the peduncle splits into the five lobes ( $\alpha, \alpha', \beta, \beta', \gamma$ )  
303 (arrowhead in **Fig. 2G,K,O**). The basis of this bulbous phenotype is unclear but may indicate that  
304 lowering levels of PCP factors in Kenyon cells that also lack Nab2 leads to a novel axon guidance defect  
305 among  $\alpha/\beta$  axons. In sum, these data reveal a pattern of dose-sensitive genetic interactions between  
306 endogenous Nab2 and PCP factors that are consistent with Nab2 modulating PCP-mediated control of  
307 MB axon projection.

308 **Nab2 is required to restrict dendritic branching and projection**

309 Loss of murine *Zc3h14* causes defects in dendritic spine morphology among hippocampal neurons  
310 (JONES *et al.* 2021) prompted us to test whether Nab2-PCP interactions in axons are also conserved in  
311 developing dendrites. For this approach, we visualized dendrites of *Drosophila* class IV dorsal dendritic  
312 arbor C (ddaC) neurons located in the larval body wall using a *pickpocket (ppk)-Gal4,UAS-GFP* system  
313 and quantified branching using Sholl intersection analysis (**Fig. 3F**) (CUNTZ *et al.* 2010). In L3 larvae,  
314 complete loss of Nab2 leads to increased dendritic branch complexity measured by the number of Scholl  
315 intersections relative to control (median of 200 in *ppk>GFP* vs. median of 252 in *Nab2<sup>ex3</sup>*; **Fig. 3A-B,G**)  
316 which is phenocopied by Nab2 RNAi depletion in ddaC neurons (median of 250 intersections in  
317 *ppk>Nab2<sup>RNAi</sup>*; **Fig. 3C,G**). Nab2 overexpression in ddaC neurons using the *Nab2<sup>EP3716</sup>* transgene has  
318 the inverse effect of decreasing Scholl intersections (median of 179 in *ppk>Nab2*; **Fig. 3E,G**).  
319 Significantly, RNAi depletion of the Wnt/PCP receptor *frizzled 2* in ddaC neurons also increases Scholl  
320 intersections (median of 216 in *ppk>fz2<sup>RNAi</sup>*; **Fig. 3D,G**), confirming prior work that Wnt/PCP signaling  
321 is involved in ddaC dendritic development (MISRA *et al.* 2016). Significantly, these effects of Nab2 loss  
322 on dendritic complexity increase with distance from the cell body (**Fig. 3H**), suggesting that the role of  
323 Nab2 in dendritic development becomes more significant with increasing distance from the cell soma.

324 The data above confirm that Nab2 and the PCP pathway are each required within ddaC neurons to  
325 guide the degree of dendritic branching. To further assess whether modulation of PCP pathway activity  
326 affects this newly defined *Nab2* dendritic role, we exploited the Matlab TREES toolbox and custom  
327 scripts to simultaneously quantify multiple dendritic phenotypes in *Nab2<sup>ex3</sup>* homozygous larvae (**Fig.**  
328 **4E**) (CUNTZ *et al.* 2010). This approach confirmed that *Nab2* loss elevates the total number of branches  
329 compared to control (**Fig. 4A,B,D**), but also revealed an extension of overall cable length (**Fig. 4A,B,C**)  
330 indicative of increased total projections. A further breakdown of *Nab2<sup>ex3</sup>* branching patterns shows an  
331 increase in maximum branch order (# of branch points along a given branch from soma to distal tip)  
332 (**Fig. 4D,F**) and coupled decrease in mean branch length (distance between consecutive branches) (**Fig.**

333 **4F)**. Thus, *Nab2<sup>ex3</sup>* ddaC arbors project and branch significantly more than control across multiple  
334 parameters (**Fig. 4F**). Due to the increased branching, *Nab2<sup>ex3</sup>* ddaC arbors exhibit reduced mean path  
335 length (-4%), smaller mean branch angles (-9%), and smaller mean branch lengths (-22%) compared to  
336 control (**Fig. 4F**). Significantly, these effects of Nab2 loss on branch and length metrics increase with  
337 distance from the cell body (**Fig. S2A-B**), which is consistent with a model in which Nab2 restriction of  
338 dendrite growth and branching is more significant with increasing distance from the cell soma.

### 339 **Planar cell polarity components dominantly modify Nab2 dendritic phenotypes.**

340 Having established that Nab2 loss elicits a spectrum of ddaC branching and projection defects, we  
341 proceeded to test whether genetic modulation of PCP activity could affect one or more of these  
342 parameters. While *Nab2<sup>ex3</sup>* homozygotes show an increase in arborization compared to controls (**Fig.**  
343 **5A-B**), single copies of the *Vang<sup>stbm6</sup>* and *Appl<sup>d</sup>* alleles (i.e., as heterozygotes) each have no significant  
344 effects on ddaC arbors in an otherwise wildtype background. In contrast, *dsh<sup>l</sup>* heterozygosity results in  
345 increased branch points, Sholl intersections, and total cable length compared to controls. When placed  
346 into the *Nab2<sup>ex3</sup>* background, single copies of *Vang<sup>stbm6</sup>* and *Appl<sup>d</sup>* alleles dominantly modify *Nab2<sup>ex3</sup>*  
347 phenotypes in opposite directions: *Vang<sup>stbm6</sup>* enhances the severity of *Nab2<sup>ex3</sup>* ddaC branching and length  
348 phenotypes while *Appl<sup>d</sup>* suppresses many of the same phenotypes (e.g., total cable length and maximum  
349 branch order; **Fig. 5I-K**). The *dsh<sup>l</sup>* allele enhances *Nab2<sup>ex3</sup>* phenotypes (**Fig. 5I-K**), although the  
350 presence of ddaC defects in *dsh<sup>l</sup>* heterozygotes suggests that this could be an additive effect.  
351 Intriguingly, use of Matlab TREES to assess branching defects as a function of distance from the cell  
352 body indicates that complexity changes induced by the *Vang<sup>stbm6</sup>* allele are primarily in *Nab2<sup>ex3</sup>* proximal  
353 arbors, while those associated with *Appl<sup>d</sup>* are primarily in distal areas of *Nab2<sup>ex3</sup>* arbors (**Fig. S2B**).  
354 Collectively, these genetic and quantitative data argue that Nab2 and PCP components are each  
355 individually required for control of ddaC arbors, and that loss of *Nab2* sensitizes ddaC development to  
356 the dosage of the core PCP component Vang and the accessory component Appl.



357 **Nab2 is required for proper Vang localization in the central complex of the brain.**

358 The pattern of genetic interactions between *Nab2* and *Vang* alleles across the axon-dendrite axis parallel  
359 the tandem mass-spectrometry (MS-MS) detection of reduced levels of Vang protein in *Nab2<sup>ex3</sup>* fly  
360 brains (**Fig. 1** and see also (CORGIAT *et al.* 2021)) and altered levels of Vangl2 protein in *Zc3h14*  
361 knockout murine brains (RHA *et al.* 2017). Given these data, we analyzed Vang protein distribution in  
362 control and *Nab2<sup>ex3</sup>* brains using a *P[acman]* genomic fragment containing the complete *Vang* locus  
363 with an *eGFP* inserted at the C-terminus of the coding sequence and retaining endogenous 5' and  
364 3'UTRs (*Vang<sup>eGFP.C</sup>*) (STRUTT *et al.* 2016). This *Vang<sup>eGFP.C</sup>* transgene rescues *Vang* loss-of-function  
365 phenotypes and thus provides a reliable readout of Vang expression patterns. Developmentally timed  
366 pupal brains were analyzed for Vang-eGFP (anti-GFP) and Bruchpilot (Brp), a presynaptic active zone  
367 protein highly enriched in the neuropil (WAGH *et al.* 2006). In control brains, Vang-eGFP fluorescence  
368 is distributed in cell bodies at the brain cortical surface as well throughout the Brp-positive central  
369 complex brain neuropil, which represents Vang in axons, dendrites, and glial processes (**Fig. 6A-B, D-**  
370 **E**). In contrast, Vang-eGFP is absent in Brp-positive neuropil regions of *Nab2<sup>ex3</sup>* brains (**Fig. 6D,F**) but  
371 is present in cortical surface cell bodies and other areas of the brain, including the intersection of the  
372 lateral anterior optic tubercle and medulla layer (NERIEC AND DESPLAN 2016; KRZEPTOWSKI *et al.* 2018;  
373 TAI *et al.* 2021) (**Fig. S4B,E**) and ventral cortical surface adjacent to the antennal lobes (WOLFF *et al.*  
374 2015; WOLFF AND RUBIN 2018) (**Fig. S4D-G**). Quantification of Vang-eGFP signal intensity in Brp-  
375 positive central neuropil ('n' box region in **Fig. 6B,E**) and a region of the dorsal cortical surface ('c' box  
376 in **Fig. 6B,E**) reveals substantial loss of neuropil-localized Vang-eGFP in *Nab2<sup>ex3</sup>* brains relative to  
377 controls, with no significant effect on the level of cortical Vang-eGFP in cell bodies (**Fig 6G-H**). Given  
378 that Brp-positive neuropil regions are enriched in axons, dendrites, and glial processes, these data  
379 indicate that Nab2 is required for Vang-eGFP protein to accumulate in distal neuronal and glial  
380 processes, and that the overall drop in Vang protein levels detected in MS-MS analysis of *Nab2<sup>ex3</sup>* brains

381 **(Fig. 1B)** is accompanied by a change in steady-state Vang-eGFP localization that may deprive distal  
382 axon-dendritic compartments of factors required for normal PCP signaling.

383 ***Zc3h14* deficient mice show PCP-like defects in the cochlea.**

384 Many phenotypes are conserved from *Nab2<sup>ex3</sup>* flies to *Zc3h14<sup>Δ13/Δ13</sup>* mice including defects in working  
385 memory (KELLY *et al.* 2016; BIENKOWSKI *et al.* 2017; RHA *et al.* 2017), a subset of proteomic changes  
386 in the brain (RHA *et al.* 2017; CORGIAT *et al.* 2021), and defects in dendritic morphology (this study and  
387 JONES *et al.* 2021). Nab2 has strong genetic interactions with PCP components, as shown here, but also  
388 has PCP-like defects in orientation of the fly wing hair bristles, a classic PCP phenotype (ADLER 2012;  
389 OLOFSSON AND AXELROD 2014; LEE *et al.* 2020). Given that mammalian ZC3H14 can rescue a variety  
390 of phenotypes when expressed in the neurons of *Nab2* mutant *Drosophila* (PAK *et al.* 2011; KELLY *et al.*  
391 2014; BIENKOWSKI *et al.* 2017), we assessed *Zc3h14<sup>Δ13/Δ13</sup>* mice for evidence of PCP defects, with a  
392 focus on elements of the sensory nervous system. Development of the organ of Corti within the cochlea  
393 is well established as a PCP-regulated process in the mouse (JONES AND CHEN 2007; CHACON-HESZELE  
394 AND CHEN 2009; RIDA AND CHEN 2009). The organ of Corti is formed by sensory cells, known as hair  
395 cells, that are patterned in one row of inner cells, and three rows of outer cells (CHACON-HESZELE AND  
396 CHEN 2009). Mutations in murine PCP genes result in altered orientation and patterning of these hair  
397 cells, due in part to the requirement for PCP in the process of convergent extension. To test whether a  
398 Nab2-PCP functional link is conserved in the mouse cochlea, we analyzed *Zc3h14<sup>Δ13/Δ13</sup>* mutant cochlea  
399 for PCP-like phenotypes. Phalloidin staining the organ of Corti from E14.5 *Zc3h14<sup>Δ13/Δ13</sup>* embryos  
400 revealed additional rows of outer hair cells (OHCs) in both the basal and middle regions compared to  
401 control (**Fig. 7A**). There are occasional inner hair cells (IHCs) patterning defects in the middle region  
402 (**Fig. 7A**). Quantification of extra cells per cochlea confirmed significant OHC patterning defects (**Fig.**  
403 **7B**) in *Zc3h14<sup>Δ13/Δ13</sup>* mice with no significant defects in IHC patterning (**Fig. 7C**). These data suggest

404 that PCP-like phenotypes are shared from *Nab2<sup>ex3</sup>* flies to *Zc3h14<sup>Δ13/Δ13</sup>* mice and that Nab2 interactions  
405 with PCP components may be conserved in ZC3H14.

406

407

408 **Discussion**

409 Here, we uncover a role for *Drosophila* Nab2, an evolutionarily conserved RBP with links to human  
410 inherited intellectual disability, in control of dendrite branching and projection among ddaC body wall  
411 sensory neurons via a mechanism that is linked to the Nab2 role in axon projection and branching via  
412 shared dependence on the PCP pathway. Loss of Nab2 increases dendrite branching and projection  
413 while overexpression of Nab2 has the opposite effect of restricting dendrite growth. Using proteomic  
414 data collected from *Nab2* null developing fly brains (CORGIAT *et al.* 2021), we uncover an enrichment  
415 for planar cell polarity factors among proteins whose steady-state levels are affected by Nab2 loss, and  
416 define a pattern of genetic interactions that are consistent with Nab2 regulating projection and branching  
417 of ddaC dendrites and MB axons by a common PCP-linked mechanism. Cell type-specific RNAi  
418 indicates that Nab2 acts cell autonomously to guide PCP-dependent axon and dendrite growth, implying  
419 a direct link between Nab2 and one or more PCP components within ddaC neurons and MB Kenyon  
420 cells. Based on reduction in levels of the PCP component Vang detected in our proteomic analysis, we  
421 analyze the levels and distribution of a fluorescently tagged Vang protein (Vang-eGFP) in adult brains  
422 (STRUTT *et al.* 2016). The overall drop in Vang-eGFP levels detected by proteomics is also evident in  
423 optical sections of whole brains and is unexpectedly accompanied by selective loss of Vang protein in  
424 axon/dendrite-enriched neuropil regions relative to brain regions containing nuclei and cell bodies.  
425 Analysis of a *Zc3h14* mutant mouse (RHA *et al.* 2017) reveals PCP phenotypes within the sensory  
426 nervous system, suggesting that functional links between Nab2/ZC3H14 and the PCP pathway may be  
427 evolutionarily conserved. Collectively, these data demonstrate that Nab2 is required to regulate axonal  
428 and dendritic growth by a PCP-linked mechanism and identify the Nab2 RBP as required for the steady-  
429 state accumulation of Vang protein in distal neuronal compartments.

430 RBP shape axon and dendrite architecture by modulating steps in post-transcriptional regulation  
431 of key neuronal mRNAs, including their export, trafficking, stability, and translation (RAVANIDIS *et al.*

432 2018; SCHIEWECK *et al.* 2021). Of note, the analysis presented here shows that effects of Nab2 on  
433 dendritic morphology are exaggerated in regions of neurons more distal from the soma as compared to  
434 more proximal regions (**Fig. 3H; Fig. S2A-B**). This enhanced effect of Nab2 loss on distal branching of  
435 ddaC arbors implies that Nab2 controls expression of an mRNA (or mRNAs) encoding a factor that  
436 guides branching and projection of more distal dendrites. While neuronal Nab2 protein is primarily  
437 nuclear (PAK *et al.* 2011), the protein is also detected in cytoplasmic messenger ribonucleoprotein  
438 (mRNP) granules and has a proposed role in translational repression (BIENKOWSKI *et al.* 2017),  
439 suggesting that cytoplasmic Nab2 could inhibit translation of mRNAs that traffic to distal dendrites and  
440 promote branching and projection. Core PCP proteins localize to membranes at distal tips of some  
441 *Drosophila* neuronal growth cones (e.g., REYNAUD *et al.* 2015; MISRA *et al.* 2016) and multiple  
442 *Drosophila* Wnt/PCP factors act autonomously in ddaC cells to control dendritic growth (e.g., *fz2* in this  
443 study and see (MATSUBARA *et al.* 2011)). Considering these observations, Nab2 might inhibit translation  
444 of one or more PCP mRNAs, perhaps as it is trafficked for subsequent expression at distal tips of axons  
445 and dendrites. The exclusion Vang-eGFP from the axon/dendrite enriched brain neuropil (**Figs. 6 and**  
446 **S4**) could then be a consequence of failed mRNA transport, followed by precocious translation (and  
447 perhaps turnover) in the soma, or it be indicative of a Nab2 role in promoting *Vang* mRNA translation in  
448 distal compartments. In sum, these data provide first evidence that *Drosophila* Nab2 may aid in  
449 localizing neurodevelopmental factors into distal dendrites, and that this may be coupled with a role in  
450 regulating mRNA trafficking and/or translation.

451 Within brain neurons, Nab2 loss depletes Vang-eGFP from neuropil, which is enriched in axons,  
452 dendrites, and glial processes and depleted of soma/nuclei (**Figs. 6 and S4**). One parsimonious model to  
453 explain this observation is that the *Vang-eGFP* mRNA is regulated by Nab2 and that Vang-eGFP  
454 depletion from *Nab2<sup>ex3</sup>* brain neuropil is thus due to a defect in *Vang-eGFP* mRNA localization and/or  
455 local translation. In this model, Nab2 could either bind directly to the *Vang* mRNA or indirectly regulate

456 *Vang* mRNA via an intermediary factor. As the *Vang*<sup>eGFP.C</sup> allele retains the single *Vang* intron and  
457 intact 5' and 3' UTRs (STRUTT *et al.* 2016), post-transcriptional regulation of the *Vang* mRNA by Nab2  
458 should be mirrored by effects on endogenous *Vang* protein, which indeed drops in abundance in *Nab2*  
459 null brains. Intriguingly, *Vang* protein is expressed in core axons of the  $\alpha$  and  $\beta$  MB lobes far from their  
460 originating Kenyon cell bodies (SHIMIZU *et al.* 2011) and is required to pattern these distal axons, as  
461 shown by the disruptive effect of *vang* loss on  $\alpha/\beta$  lobe structure (SHIMIZU *et al.* 2011; NG 2012). Thus,  
462 the interactions between *Nab2* and *Vang* alleles in MB axons may also reflect a specific role for both  
463 factors in controlling projection and branching of distal neuronal processes that mirrors their relationship  
464 in ddaC dendrites.

465 The genetic interactions between *Nab2* and alleles of PCP components in MB axons imply a  
466 degree of context-dependence to the Nab2-PCP interaction between ddaCs and MBs, and even between  
467 the two distinct axon compartments represented by the MB  $\alpha$ - and  $\beta$ -lobes. While *Vang*<sup>sbm6</sup>  
468 heterozygosity enhances *Nab2*<sup>ex3</sup> ddaC defects, this allele selectively suppresses *Nab2*<sup>ex3</sup> MB  $\alpha$ -lobe  
469 defects but not  $\beta$ -lobe defects. Given the broad drop in *Vang*-eGFP levels observed in *Nab2*<sup>ex3</sup> brains  
470 (**Fig. 6**), and the requirement for *Vang* in Kenyon cells (KCs) for normal development of both the  $\alpha$  and  
471  $\beta$ -lobes (SHIMIZU *et al.* 2011; NG 2012), the  $\alpha$ -lobe-specific *Nab2-Vang* genetic interaction could be  
472 regarded as unexpected. However, very similar  $\alpha$ -lobe-specific genetic interactions occur between *Nab2*  
473 and alleles of two other RBP genes, *fmr1* and *Atx2* (BIENKOWSKI *et al.* 2017; ROUNDS 2021), implying  
474 that Nab2 has distinct interacting pathways in these two different axonal sub-compartments. As noted,  
475 suppression of *Nab2*<sup>ex3</sup> MB defects by *Vang*<sup>sbm6</sup> is the inverse of how this same allele affects *Nab2*<sup>ex3</sup>  
476 ddaC phenotypes. The relationship could arise if PCP signals are exchanged between MB axons and the  
477 surrounding neuro-substrate, which could invert a relationship between Nab2 in Kenyon cells and  
478 Wnt/PCP signals emanating from surrounding cells. For example, the receptor *derailed* is expressed in  
479 the dorsomedial lineage neuropil and binds Wnt5 for presentation to repulsive *derailed2* receptors on  $\alpha$ -

480 lobe axons, thus non-autonomously guiding  $\alpha$ -lobe projection (REYNAUD *et al.* 2015). In addition, the  
481 projection paths of individual *vang*<sup>stbm6</sup> mutant  $\alpha$  and  $\beta$ -axon tracts can be rescued by adjacent cells with  
482 normal Vang level, indicating that Wnt/PCP control of  $\alpha$  and  $\beta$ -axon branching is not strictly cell-  
483 autonomous (SHIMIZU *et al.* 2011; NG 2012). These complex signaling relationships within MB axons,  
484 and potential extra-cellular Wnt/PCP guidance cues emanating from surrounding dorsomedial cells, are  
485 both potential explanations for context-specific genetic interactions between *Nab2* and *Vang* in ddaCs  
486 and Kenyon cells. In contrast to *Vang* alleles, partial loss of *Appl* (*Appl*<sup>d</sup>) consistently suppresses both  
487 *Nab2*<sup>ex3</sup> dendritic and axonal phenotypes (**Fig. S3**) which parallels the increase in *Appl* protein detected  
488 in brain proteomics in *Nab2* mutant brains (**Fig. 1B, Table S1**). *Appl* acts as a downstream neuronal-  
489 specific effector of the PCP pathway (SOLDANO *et al.* 2013; LIU *et al.* 2021) and elevated *Appl* protein  
490 in response to *Nab2* loss could be an indirect consequence of altered core PCP pathway activity or  
491 evidence of direct regulation of the *Appl* transcript. These differing interactions illustrate the complexity  
492 of RBP function across a neuron with specific interactions affecting sub-cellular compartments in  
493 different ways.

494 An additional question that arises from analysis of *Nab2*-PCP interactions in the MBs is: *why*  
495 *Nab2* mutant  $\alpha$ -lobe defects are rescued by *Vang*, *Appl*, and *dsh* alleles to a greater degree than are  $\beta$ -  
496 lobe defects? As noted above, alleles of the *Nab2*-interacting factors *fmr1* and *Atx2* also specifically  
497 suppress *Nab2*<sup>ex3</sup>  $\alpha$ -axon defects but not  $\beta$ -axon defects (BIENKOWSKI *et al.* 2017), implying that these  
498 gene may define a *Nab2*-dependent  $\alpha$ -lobe *Nab2*-*Fmr1*-*Atx2* regulatory network that also includes PCP  
499 mRNAs. Indeed, *fmr1* also shares some functional features with *Nab2* in MBs and ddaCs: *Fmr1* controls  
500 both  $\alpha$ - and  $\beta$ -lobe development (MICHEL *et al.* 2004) and limits ddaC dendrite development, in part  
501 through an interaction the mRNA encoding the PCP-effector *Rac1* (FANTO *et al.* 2000; LEE *et al.* 2003).  
502 Significantly, the normal development of  $\alpha$  and  $\beta$ -axons has been proposed to rely on a lobe-specific  
503 PCP mechanism involving the formin DAAM (Dsh associated activator of morphogenesis) interacting

504 with Wg/Wnt receptor Frizzled (Fz) in the  $\alpha$ -lobes and Vang in the  $\beta$ -lobes (GOMBOS *et al.* 2015). A  
505 similar type of mechanism could occur for the Nab2-PCP interaction, with Nab2 either regulating  
506 different PCP components in  $\alpha$  vs.  $\beta$  lobes or regulating components that themselves have lobe-specific  
507 roles e.g., DAAM or the Derailed-Wnt5 receptor ligand pair (REYNAUD *et al.* 2015). In sum, it seems  
508 likely that future studies will identify other mechanisms and pathways through which Nab2 regulates  
509 axon-dendrite development in opposition to or cooperation with the Wnt/PCP pathway, including for  
510 example mechanisms involving the Fmr1 and Atx2 RBPs interacting with Nab2 to regulate expression  
511 of co-bound RNAs.

512 We extended the data from *Drosophila* to mouse by taking advantage of a mouse model lacking  
513 functional ZC3H14/Nab2 protein (RHA *et al.* 2017). This analysis reveals that *zc3h14* mutant mice show  
514 phenotypes in orientation of the hair cell stereociliary bundles within the cochlea that are similar to  
515 multiple PCP mutants, including *Vangl2* (MONTCOUQUIOL *et al.* 2003). Future studies could employ  
516 mouse models to explore whether genetic interactions identified in *Drosophila* extend to mammals, but  
517 this conserved PCP phenotype argues for a conserved link between ZC3H14/Nab2 and the PCP  
518 pathway.

519 In aggregate, these data reveal Nab2 interactions with the PCP pathway and provide the first  
520 evidence that Nab2 is required for dendritic development. These interactions between Nab2 and PCP  
521 factors in control of dendritic complexity and MB axon projection appear to be cell-autonomous and, at  
522 least in ddaC arbors, more dramatic in distal projections. Changes in expression level and localization of  
523 Vang protein in fly brains lacking Nab2 highlight the *Vang* mRNA as a potential target of post-  
524 transcriptional control by Nab2 both in axons and dendrites. Given that loss of the Nab2 ortholog in  
525 mice, *Zc3h14*, also alters levels of the *Vangl2* PCP protein in the adult hippocampus, and that mutations  
526 in PCP genes including *Vangl2* are linked to intellectual disabilities, severe neural tube closure defects,  
527 and microencephaly in humans (e.g., WANG *et al.* 2019) dysregulation of the levels and localization of



Corgiat et al.

528 PCP components in neurons is one potential mechanism to explain axonal and dendritic phenotypes in  
529 *Zc3h14* mutant mice (JONES *et al.* 2021) and cognitive defects in human patients lacking ZC3H14 (PAK  
530 *et al.* 2011).

531

532 **Acknowledgements:** We thank Dr. Dan Cox, GA State Neuroscience Institute, for reagents and  
533 discussion, and members of the Moberg and Corbett laboratories for helpful discussions. We thank the  
534 Emory Proteomics Core for their support and guidance.

535 **Data availability:** Proteomics data have been deposited to the ProteomeXchange Consortium via the  
536 PRIDE partner repository with the dataset identifier PXD022984. All remaining data are contained  
537 within the article.

538 **Funding and additional information:** Research reported in this publication was also supported in part  
539 by the Emory University Integrated Cellular Imaging Microscopy Core of the Emory Neuroscience  
540 NINDS Core Facilities grant, 5P30NS055077. Financial support as follows: 5F31NS110312,  
541 5F31HD088043, and 5R01MH107305.

542 The authors declare no competing financial interests.

543

544

545

546 **Figure legends:**

547

548 **Figure 1: Nab2 loss alters levels of planar cell polarity pathway proteins in the *Drosophila* brain.**

549 (A) Schematic summary of quantitative proteomic analysis of *Nab2<sup>ex3</sup>* pupal brains dissected from  
550 *control* or *Nab2<sup>ex3</sup>* pupa 24.5 hours after puparium formation. Ten samples per genotype, each composed  
551 of 20 brains (i.e., 200 *control* brains and 200 *Nab2<sup>ex3</sup>* brains) were processed and analyzed using an  
552 Orbitrap Fusion Tribrid Mass Spectrometer and data was quantified using MaxQuant against the  
553 *Drosophila melanogaster* Uniprot database. (B) Chord plot analysis of protein abundance changes in  
554 *Nab2<sup>ex3</sup>* relative to *control* for selected color-coded planar cell polarity ontology terms. Heat map  
555 indicates fold-change in abundance of each protein ( $\log_2(Nab2^{ex3}/control)$ ); blue=decreased,  
556 red=increased.

557 **Figure 2: Planar cell polarity components dominantly modify Nab2 axonal phenotypes.**

558 Paired maximum intensity Z-stack projections images and single transverse sections of anti-Fasciclin II  
559 (FasII) stained 48-72hr pupal brains from (A-B) *control* or (C-D) *Nab2<sup>ex3</sup>* animals, or each of these  
560 genotypes combined with (E-H) *Vang<sup>stbm6/+</sup>*, (I-L) *App1<sup>d/+</sup>*, or (M-P) *dsh<sup>1/+</sup>*. Frequencies of (Q)  $\alpha$ -  
561 lobe or (R)  $\beta$ -lobe structure defects in these genotypes using the scoring system as described in  
562 Experimental Procedures. *Nab2<sup>ex3</sup>* brains show high penetrance thinning/loss of  $\alpha$ -lobes (85%) and  
563 fusion/missing of  $\beta$ -lobe (88%) which are dominantly suppressed by *Vang<sup>stbm-6</sup>* (49%  $\alpha$ -lobe and 33%  $\beta$ -  
564 lobe defects), *App1<sup>d</sup>* (62%  $\alpha$ -lobe and 35%  $\beta$ -lobe defects). *dsh<sup>1</sup>* selectively suppress *Nab2<sup>ex3</sup>*  $\alpha$ -lobe  
565 defects to 63%.

566 **Figure 3: Nab2 is required for proper dendritic development.**

567 Inverted intensity images of *Drosophila* class IV dorsal dendritic arbor C (ddaC) neurons from (A)  
568 *pickpocket (ppk)-Gal4,UAS-GFP*, (B) *Nab2<sup>ex3</sup>*, (C) *ppk-Gal4,UAS-GFP,Nab2<sup>RNAi</sup>*, (D) *ppk-Gal4,UAS-*  
569 *GFP,fz2<sup>RNAi</sup>*, and (E) *ppk-Gal4,UAS-GFP,Nab2<sup>oe</sup>* L3 larvae. Inset black boxes show high magnification  
570 views of dendritic arbors. (F) Diagram depicting the concentric rings used to perform Sholl analysis

571 overlaid on the dendritic arbor of a neuron. The half of the rings proximal to the soma labeled in blue;  
572 the half of the rings distal to the soma labeled in red. **(G-H)** Quantification of branching complexity by  
573 Sholl analysis of total intersections across dendritic arbor; bars represent median and upper/lower  
574 quartile, \*  $p < 0.05$ . **(G)** Sholl analysis of full dendritic arbor. Median Sholl intersection values are 200 in  
575 *ppk-Gal4,UAS-GFP* (n=32), 252 in *Nab2<sup>ex3</sup>* (n=17), 250 in *ppk-Gal4,UAS-GFP,Nab2<sup>RNAi</sup>* (n=12), 216 in  
576 *ppk-Gal4,UAS-fz<sup>RNAi</sup>* (n=12), and 179 in *ppk-Gal4,UAS-Nab2<sup>oe</sup>* (n=15). **(H)** Sholl analysis of proximal  
577 and distal dendritic arbors. Median Sholl intersection values for *ppk-Gal4,UAS-GFP* (n=32) are 96  
578 proximal and 108.5 distal, while median Sholl intersection values for *Nab2<sup>ex3</sup>* are 102 proximal and 141  
579 distal.

580 **Figure 4: Nab2 restricts dendritic branching and projection.**

581 Inverted intensity images of *Drosophila* class IV dorsal dendritic arbor C (ddaC) neurons from **(A)**  
582 *control* +/+, **(B)** *Nab2<sup>ex3</sup>* larvae. Inset black boxes show high magnification views of dendritic arbors.  
583 Quantification of **(C)** total cable length and **(D)** maximum branch order for *control* (n=32) and *Nab2<sup>ex3</sup>*  
584 (n=17); bars represent median and upper/lower quartile, \*  $p < 0.05$ . **(E)** Schematic depicting measured  
585 dendritic parameters using Matlab TREES toolbox and custom scripts. **(F)** Balloon plot depicting ten  
586 measurements of the *Nab2<sup>ex3</sup>* dendritic arbor. Heat map shows change percent changes in *Nab2<sup>ex3</sup>* vs  
587 *control*.

588 **Figure 5: Planar cell polarity components dominantly modify Nab2 dendritic phenotypes.**

589 Inverted intensity images of *Drosophila* class IV dorsal dendritic arbor C (ddaC) neurons from **(A)**  
590 *control* +/+ or **(B)** *Nab2<sup>ex3</sup>* larvae alone, or in combination with **(C-D)** *Vang<sup>stbm6</sup>/+*, **(E-F)** *Appl<sup>d</sup>/+*, **(G-**  
591 **H)** *dsh<sup>l</sup>/+*. Inset black boxes show high magnification views of dendritic arbors. **(I-J)** Quantification of  
592 **(I)** total cable length and **(J)** maximum branch order in the indicated genotypes; errors bars represent  
593 median and upper/lower quartile, \*  $p < 0.05$ . **(K)** Balloon plot analysis of 10 arbor parameters in the

594 indicated genotypes. Heat map shows change percent changes in *Nab2<sup>ex3</sup>* vs *control*. Significance  
595 depicted by balloon size (large balloon =  $p < 0.05$ , small balloon = ns).

596 **Figure 6: Nab2 is required for proper Vang localization in the central complex of the brain.**

597 Visualization of brains from 48-72hr *vang<sup>EGFP.C</sup>* (A-C) and *Nab2<sup>ex3</sup>;vang<sup>EGFP.C</sup>* (D-F) pupae co-stained  
598 with anti-GFP (green) and the nc82 mAb (red) to detect Vang-eGFP and Brp, which marks presynaptic  
599 actives zones. Dashed boxes indicate regions used for quantifying fluorescence in **c** (cortical surface)  
600 and **n** (central neuropil) regions. (G-H) Quantification of Vang-eGFP fluorescence intensity in the (G)  
601 cortical surface and (H) central neuropil regions of *vang<sup>EGFP.C</sup>* (n=9) and *Nab2<sup>ex3</sup>;vang<sup>EGFP.C</sup>* (n=9)  
602 pupae. Bars represent median and upper/lower quartile, \*  $p < 0.05$ .

603 **Figure 7: *Zc3h14<sup>Δ13/Δ13</sup>* mice have PCP-like cochlear defects.**

604 (A) The cochlea from *control* and *Zc3h14<sup>Δ13/Δ13</sup>* E14.5 embryos showing basal and middle regions.  
605 Stereocilia are visualized by phalloidin staining. Brackets indicate outer hair cells (OHC) and  
606 arrowheads indicate inner hair cells (IHC). Staining reveals normal orientation and hair cell layers for  
607 *control* but extra OHC and some orientation defects around the pillar cell region for *Zc3h14<sup>Δ13/Δ13</sup>*. (B-C)  
608 Quantification of extra cells per cochlea in the (B) OHC and (C) IHC; bars represent median and  
609 upper/lower quartile, \* indicates  $p < 0.05$ . *control* n=4, *Zc3h14<sup>Δ13/Δ13</sup>* n=4.

610

611

612

613 **Bibliography**

- 614
- 615 Adler, P. N., 2012 The frizzled/stan pathway and planar cell polarity in the Drosophila wing. *Curr Top*
- 616 *Dev Biol* 101: 1-31. doi:10.1016/B978-0-12-394592-1.00001-6
- 617 Adler, P. N., and J. B. Wallingford, 2017 From Planar Cell Polarity to Ciliogenesis and Back: The
- 618 Curious Tale of the PPE and CPLANE proteins. *Trends Cell Biol* 27: 379-390.
- 619 doi:10.1016/j.tcb.2016.12.001
- 620 Agrawal, S., P. H. Kuo, L. Y. Chu, B. Golzarroshan, M. Jain *et al.*, 2019 RNA recognition motifs of
- 621 disease-linked RNA-binding proteins contribute to amyloid formation. *Sci Rep* 9: 6171.
- 622 doi:10.1038/s41598-019-42367-8
- 623 Alboukadel, K., 2018 *ggpubr: "ggplot2" based publication ready plots. R Package Ver. 0.2*
- 624 Alpatov, R., B. J. Lesch, M. Nakamoto-Kinoshita, A. Blanco, S. Chen *et al.*, 2014 A chromatin-
- 625 dependent role of the fragile X mental retardation protein FMRP in the DNA damage response.
- 626 *Cell* 157: 869-881. doi:10.1016/j.cell.2014.03.040
- 627 Andre, P., Q. Wang, N. Wang, B. Gao, A. Schilit *et al.*, 2012 The Wnt coreceptor Ryk regulates
- 628 Wnt/planar cell polarity by modulating the degradation of the core planar cell polarity
- 629 component Vangl2. *J Biol Chem* 287: 44518-44525. doi:10.1074/jbc.M112.414441
- 630 Bala Tannan, N., G. Collu, A. C. Humphries, E. Serysheva, U. Weber *et al.*, 2018 AKAP200 promotes
- 631 Notch stability by protecting it from Cbl/lysosome-mediated degradation in Drosophila
- 632 melanogaster. *PLoS Genet* 14: e1007153. doi:10.1371/journal.pgen.1007153
- 633 Bienkowski, R. S., A. Banerjee, J. C. Rounds, J. Rha, O. F. Omotade *et al.*, 2017 The Conserved,
- 634 Disease-Associated RNA Binding Protein dNab2 Interacts with the Fragile X Protein Ortholog in
- 635 Drosophila Neurons. *Cell Rep* 20: 1372-1384. doi:10.1016/j.celrep.2017.07.038
- 636 Boutros, M., and M. Mlodzik, 1999 Dishevelled: at the crossroads of divergent intracellular signaling
- 637 pathways. *Mech Dev* 83: 27-37. doi:10.1016/s0925-4773(99)00046-5
- 638 Cang, J., and D. A. Feldheim, 2013 Developmental mechanisms of topographic map formation and
- 639 alignment. *Annu Rev Neurosci* 36: 51-77. doi:10.1146/annurev-neuro-062012-170341
- 640 Chacon-Heszele, M. F., and P. Chen, 2009 Mouse models for dissecting vertebrate planar cell polarity
- 641 signaling in the inner ear. *Brain Res* 1277: 130-140. doi:10.1016/j.brainres.2009.02.004
- 642 Chen, E. Y., C. M. Tan, Y. Kou, Q. Duan, Z. Wang *et al.*, 2013 Enrichr: interactive and collaborative
- 643 HTML5 gene list enrichment analysis tool. *BMC Bioinformatics* 14: 128. doi:10.1186/1471-
- 644 2105-14-128
- 645 Clark, S. G., L. L. Graybeal, S. Bhattacharjee, C. Thomas, S. Bhattacharya *et al.*, 2018 Basal autophagy
- 646 is required for promoting dendritic terminal branching in Drosophila sensory neurons. *PLoS One*
- 647 13: e0206743. doi:10.1371/journal.pone.0206743
- 648 Corgiat, E. B., S. M. List, J. C. Rounds, A. H. Corbett and K. H. Moberg, 2021 The RNA binding
- 649 protein Nab2 regulates the proteome of the developing Drosophila brain. *J Biol Chem*: 100877.
- 650 doi:10.1016/j.jbc.2021.100877
- 651 Courbard, J. R., A. Djiane, J. Wu and M. Mlodzik, 2009 The apical/basal-polarity determinant Scribble
- 652 cooperates with the PCP core factor Stbm/Vang and functions as one of its effectors. *Dev Biol*
- 653 333: 67-77. doi:10.1016/j.ydbio.2009.06.024
- 654 Cuntz, H., F. Forstner, A. Borst and M. Hausser, 2010 One rule to grow them all: a general theory of
- 655 neuronal branching and its practical application. *PLoS Comput Biol* 6.
- 656 doi:10.1371/journal.pcbi.1000877
- 657 Edens, B. M., S. Ajroud-Driss, L. Ma and Y. C. Ma, 2015 Molecular mechanisms and animal models of
- 658 spinal muscular atrophy. *Biochim Biophys Acta* 1852: 685-692.
- 659 doi:10.1016/j.bbadis.2014.07.024

- 660 Engel, K. L., A. Arora, R. Goering, H. G. Lo and J. M. Taliaferro, 2020 Mechanisms and consequences  
661 of subcellular RNA localization across diverse cell types. *Traffic* 21: 404-418.  
662 doi:10.1111/tra.12730
- 663 Fagan, J. K., G. Dollar, Q. Lu, A. Barnett, J. Pechuan Jorge *et al.*, 2014 Combover/CG10732, a novel  
664 PCP effector for Drosophila wing hair formation. *PLoS One* 9: e107311.  
665 doi:10.1371/journal.pone.0107311
- 666 Fanto, M., U. Weber, D. I. Strutt and M. Mlodzik, 2000 Nuclear signaling by Rac and Rho GTPases is  
667 required in the establishment of epithelial planar polarity in the Drosophila eye. *Curr Biol* 10:  
668 979-988. doi:10.1016/s0960-9822(00)00645-x
- 669 Gebauer, F., T. Schwarzl, J. Valcarcel and M. W. Hentze, 2021 RNA-binding proteins in human genetic  
670 disease. *Nat Rev Genet* 22: 185-198. doi:10.1038/s41576-020-00302-y
- 671 Gombos, R., E. Migh, O. Antal, A. Mukherjee, A. Jenny *et al.*, 2015 The Formin DAAM Functions as  
672 Molecular Effector of the Planar Cell Polarity Pathway during Axonal Development in  
673 Drosophila. *J Neurosci* 35: 10154-10167. doi:10.1523/JNEUROSCI.3708-14.2015
- 674 Goodrich, L. V., and D. Strutt, 2011 Principles of planar polarity in animal development. *Development*  
675 138: 1877-1892. doi:10.1242/dev.054080
- 676 Gross, C., E. M. Berry-Kravis and G. J. Bassell, 2012 Therapeutic strategies in fragile X syndrome:  
677 dysregulated mGluR signaling and beyond. *Neuropsychopharmacology* 37: 178-195.  
678 doi:10.1038/npp.2011.137
- 679 Gross, G. G., G. M. Lone, L. K. Leung, V. Hartenstein and M. Guo, 2013 X11/Mint genes control  
680 polarized localization of axonal membrane proteins in vivo. *J Neurosci* 33: 8575-8586.  
681 doi:10.1523/JNEUROSCI.5749-12.2013
- 682 Hagiwara, A., M. Yasumura, Y. Hida, E. Inoue and T. Ohtsuka, 2014 The planar cell polarity protein  
683 Vangl2 bidirectionally regulates dendritic branching in cultured hippocampal neurons. *Mol Brain*  
684 7: 79. doi:10.1186/s13041-014-0079-5
- 685 Hindges, R., T. McLaughlin, N. Genoud, M. Henkemeyer and D. O'Leary, 2002 EphB forward signaling  
686 controls directional branch extension and arborization required for dorsal-ventral retinotopic  
687 mapping. *Neuron* 35: 475-487. doi:10.1016/s0896-6273(02)00799-7
- 688 Holt, C. E., K. C. Martin and E. M. Schuman, 2019 Local translation in neurons: visualization and  
689 function. *Nat Struct Mol Biol* 26: 557-566. doi:10.1038/s41594-019-0263-5
- 690 Hornberg, H., and C. Holt, 2013 RNA-binding proteins and translational regulation in axons and growth  
691 cones. *Front Neurosci* 7: 81. doi:10.3389/fnins.2013.00081
- 692 Iyer, S. C., E. P. Ramachandran Iyer, R. Meduri, M. Rubaharan, A. Kuntimaddi *et al.*, 2013 Cut, via  
693 CrebA, transcriptionally regulates the COPII secretory pathway to direct dendrite development in  
694 Drosophila. *J Cell Sci* 126: 4732-4745. doi:10.1242/jcs.131144
- 695 Jackson, S. M., and C. A. Berg, 2002 An A-kinase anchoring protein is required for protein kinase A  
696 regulatory subunit localization and morphology of actin structures during oogenesis in  
697 Drosophila. *Development* 129: 4423-4433
- 698 Jones, C., and P. Chen, 2007 Planar cell polarity signaling in vertebrates. *Bioessays* 29: 120-132.  
699 doi:10.1002/bies.20526
- 700 Jones, S. K., J. Rha, S. Kim, K. J. Morris, O. F. Omotade *et al.*, 2021 The Polyadenosine RNA Binding  
701 Protein ZC3H14 is Required in Mice for Proper Dendritic Spine Density. *bioRxiv*
- 702 Jones, W. M., A. T. Chao, M. Zavortink, R. Saint and A. Bejsovec, 2010 Cytokinesis proteins Tum and  
703 Pav have a nuclear role in Wnt regulation. *J Cell Sci* 123: 2179-2189. doi:10.1242/jcs.067868
- 704 Jung, H., B. C. Yoon and C. E. Holt, 2012 Axonal mRNA localization and local protein synthesis in  
705 nervous system assembly, maintenance and repair. *Nat Rev Neurosci* 13: 308-324.  
706 doi:10.1038/nrn3210

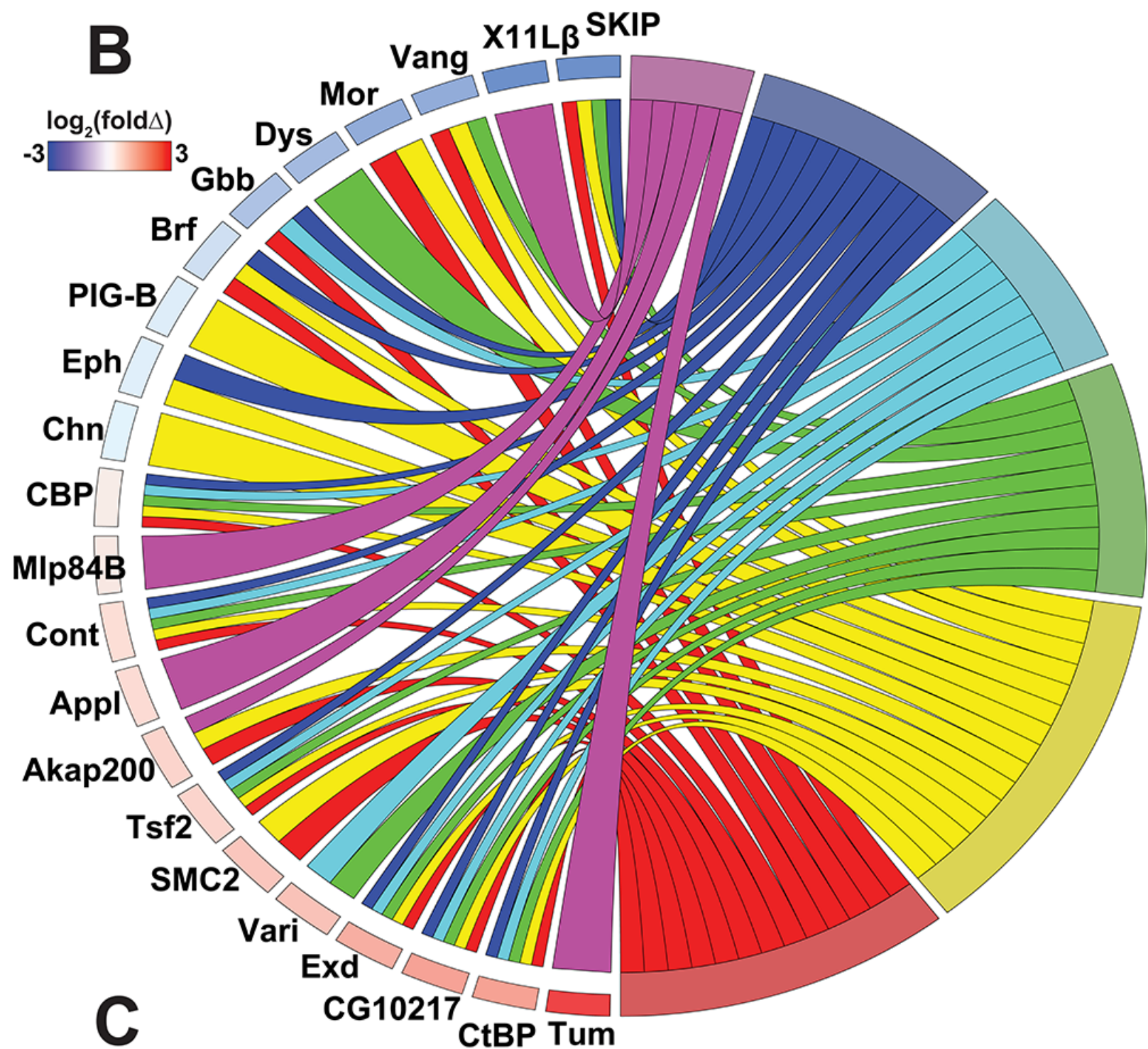
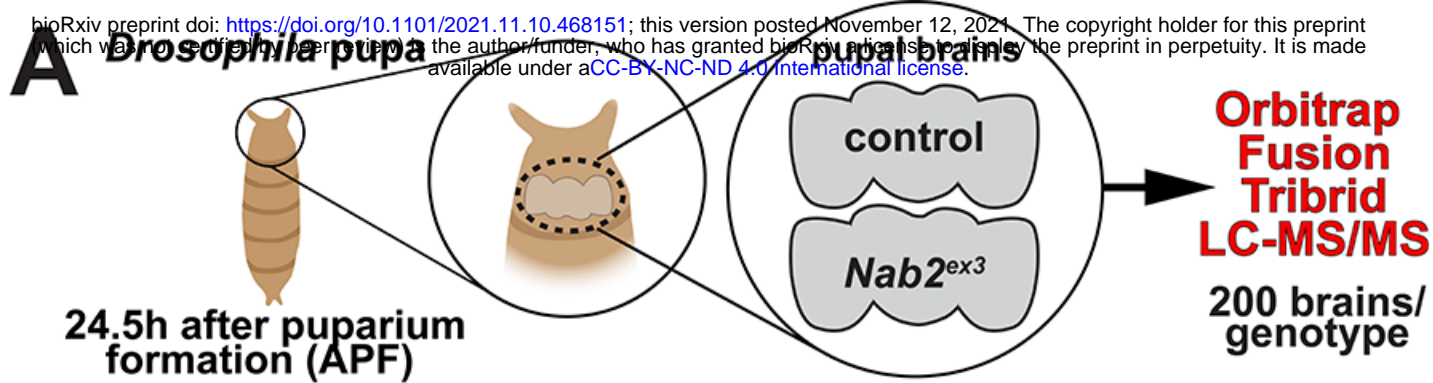
- 707 Kelly, S. M., R. Bienkowski, A. Banerjee, D. J. Melicharek, Z. A. Brewer *et al.*, 2016 The *Drosophila*  
708 ortholog of the Zc3h14 RNA binding protein acts within neurons to pattern axon projection in  
709 the developing brain. *Dev Neurobiol* 76: 93-106. doi:10.1002/dneu.22301
- 710 Kelly, S. M., S. W. Leung, C. Pak, A. Banerjee, K. H. Moberg *et al.*, 2014 A conserved role for the zinc  
711 finger polyadenosine RNA binding protein, ZC3H14, in control of poly(A) tail length. *RNA* 20:  
712 681-688. doi:10.1261/rna.043984.113
- 713 Krzeptowski, W., L. Walkowicz, A. Plonczynska and J. Gorska-Andrzejak, 2018 Different Levels of  
714 Expression of the Clock Protein PER and the Glial Marker REPO in Ensheathing and Astrocyte-  
715 Like Glia of the Distal Medulla of *Drosophila* Optic Lobe. *Front Physiol* 9: 361.  
716 doi:10.3389/fphys.2018.00361
- 717 Kuleshov, M. V., J. E. L. Diaz, Z. N. Flamholz, A. B. Keenan, A. Lachmann *et al.*, 2019 modEnrichr: a  
718 suite of gene set enrichment analysis tools for model organisms. *Nucleic Acids Res* 47: W183-  
719 W190. doi:10.1093/nar/gkz347
- 720 Kuleshov, M. V., M. R. Jones, A. D. Rouillard, N. F. Fernandez, Q. Duan *et al.*, 2016 Enrichr: a  
721 comprehensive gene set enrichment analysis web server 2016 update. *Nucleic Acids Res* 44:  
722 W90-97. doi:10.1093/nar/gkw377
- 723 Lee, A., W. Li, K. Xu, B. A. Bogert, K. Su *et al.*, 2003 Control of dendritic development by the  
724 *Drosophila* fragile X-related gene involves the small GTPase Rac1. *Development* 130: 5543-  
725 5552. doi:10.1242/dev.00792
- 726 Lee, W. H., E. Corgiat, J. C. Rounds, Z. Shepherd, A. H. Corbett *et al.*, 2020 A Genetic Screen Links  
727 the Disease-Associated Nab2 RNA-Binding Protein to the Planar Cell Polarity Pathway in  
728 *Drosophila melanogaster*. *G3 (Bethesda)* 10: 3575-3583. doi:10.1534/g3.120.401637
- 729 Liu, T., T. Zhang, M. Nicolas, L. Boussicault, H. Rice *et al.*, 2021 The amyloid precursor protein is a  
730 conserved Wnt receptor. *Elife* 10. doi:10.7554/eLife.69199
- 731 Maechler, M., P. Rousseeuw, A. Struyf, M. Hubert, M. Studer *et al.*, 2016 *cluster: Cluster Analysis*  
732 *Basics and Extensions*.
- 733 Matsubara, D., S. Y. Horiuchi, K. Shimono, T. Usui and T. Uemura, 2011 The seven-pass  
734 transmembrane cadherin Flamingo controls dendritic self-avoidance via its binding to a LIM  
735 domain protein, Espinas, in *Drosophila* sensory neurons. *Genes Dev* 25: 1982-1996.  
736 doi:10.1101/gad.16531611
- 737 Mattioli, F., E. Schaefer, A. Magee, P. Mark, G. M. Mancini *et al.*, 2017 Mutations in Histone Acetylase  
738 Modifier BRPF1 Cause an Autosomal-Dominant Form of Intellectual Disability with Associated  
739 Ptois. *Am J Hum Genet* 100: 105-116. doi:10.1016/j.ajhg.2016.11.010
- 740 McLaughlin, T., and D. D. O'Leary, 2005 Molecular gradients and development of retinotopic maps.  
741 *Annu Rev Neurosci* 28: 327-355. doi:10.1146/annurev.neuro.28.061604.135714
- 742 Michel, C. I., R. Kraft and L. L. Restifo, 2004 Defective neuronal development in the mushroom bodies  
743 of *Drosophila* fragile X mental retardation 1 mutants. *J Neurosci* 24: 5798-5809.  
744 doi:10.1523/JNEUROSCI.1102-04.2004
- 745 24/25/5798 [pii]
- 746 Misra, M., H. Edmund, D. Ennis, M. A. Schlueter, J. E. Marot *et al.*, 2016 A Genome-Wide Screen for  
747 Dendritically Localized RNAs Identifies Genes Required for Dendrite Morphogenesis. *G3*  
748 (*Bethesda*) 6: 2397-2405. doi:10.1534/g3.116.030353
- 749 Mlodzik, M., 2020 Planar cell polarity: moving from single cells to tissue-scale biology. *Development*  
750 147. doi:10.1242/dev.186346
- 751 Montcouquiol, M., R. A. Rachel, P. J. Lanford, N. G. Copeland, N. A. Jenkins *et al.*, 2003 Identification  
752 of Vangl2 and Scrb1 as planar polarity genes in mammals. *Nature* 423: 173-177.  
753 doi:10.1038/nature01618



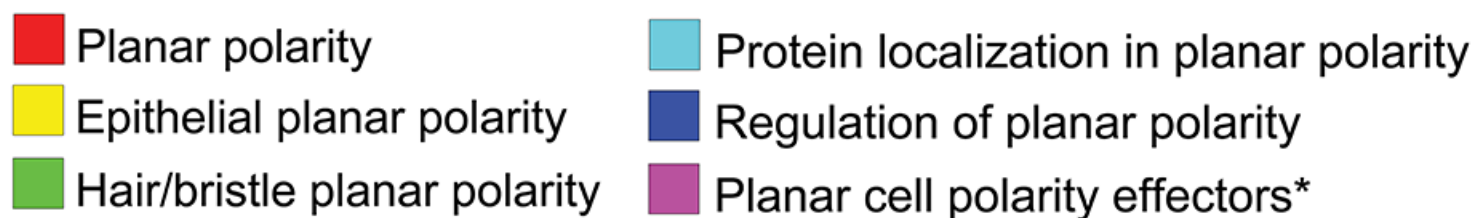
- 754 Neriec, N., and C. Desplan, 2016 From the Eye to the Brain: Development of the Drosophila Visual  
755 System. *Curr Top Dev Biol* 116: 247-271. doi:10.1016/bs.ctdb.2015.11.032
- 756 Ng, J., 2012 Wnt/PCP proteins regulate stereotyped axon branch extension in Drosophila. *Development*  
757 139: 165-177. doi:10.1242/dev.068668
- 758 Olofsson, J., and J. D. Axelrod, 2014 Methods for studying planar cell polarity. *Methods* 68: 97-104.  
759 doi:10.1016/j.ymeth.2014.03.017
- 760 Pak, C., M. Garshasbi, K. Kahrizi, C. Gross, L. H. Apponi *et al.*, 2011 Mutation of the conserved  
761 polyadenosine RNA binding protein, ZC3H14/dNab2, impairs neural function in Drosophila and  
762 humans. *Proc Natl Acad Sci U S A* 108: 12390-12395. doi:1107103108 [pii]  
763 10.1073/pnas.1107103108
- 764 Peng, Y., and J. D. Axelrod, 2012 Asymmetric protein localization in planar cell polarity: mechanisms,  
765 puzzles, and challenges. *Curr Top Dev Biol* 101: 33-53. doi:10.1016/B978-0-12-394592-  
766 1.00002-8
- 767 Puram, S. V., and A. Bonni, 2013 Cell-intrinsic drivers of dendrite morphogenesis. *Development* 140:  
768 4657-4671. doi:10.1242/dev.087676
- 769 Qian, D., C. Jones, A. Rzdzinska, S. Mark, X. Zhang *et al.*, 2007 Wnt5a functions in planar cell  
770 polarity regulation in mice. *Dev Biol* 306: 121-133. doi:10.1016/j.ydbio.2007.03.011
- 771 R-Team, D. C., 2018 R: A language and environment for statistical computing. *R Found. Stat. Compt.*
- 772 Radde-Gallwitz, K., L. Pan, L. Gan, X. Lin, N. Segil *et al.*, 2004 Expression of Islet1 marks the sensory  
773 and neuronal lineages in the mammalian inner ear. *J Comp Neurol* 477: 412-421.  
774 doi:10.1002/cne.20257
- 775 Ravanidis, S., F. G. Kattan and E. Doxakis, 2018 Unraveling the Pathways to Neuronal Homeostasis and  
776 Disease: Mechanistic Insights into the Role of RNA-Binding Proteins and Associated Factors.  
777 *Int J Mol Sci* 19. doi:10.3390/ijms19082280
- 778 Reynaud, E., L. L. Lahaye, A. Boulanger, I. M. Petrova, C. Marquilly *et al.*, 2015 Guidance of  
779 Drosophila Mushroom Body Axons Depends upon DRL-Wnt Receptor Cleavage in the Brain  
780 Dorsomedial Lineage Precursors. *Cell Rep* 11: 1293-1304. doi:10.1016/j.celrep.2015.04.035
- 781 Rha, J., S. K. Jones, J. Fidler, A. Banerjee, S. W. Leung *et al.*, 2017 The RNA-binding Protein,  
782 ZC3H14, is Required for Proper Poly(A) Tail Length Control, Expression of Synaptic Proteins,  
783 and Brain Function in Mice. *Hum Mol Genet.* doi:10.1093/hmg/ddx248
- 784 Rida, P. C., and P. Chen, 2009 Line up and listen: Planar cell polarity regulation in the mammalian inner  
785 ear. *Semin Cell Dev Biol* 20: 978-985. doi:10.1016/j.semcdb.2009.02.007
- 786 Rounds, J. C., Corgiat, E. B., Ye, C., Behnke, J. A., Kelly, S. M., Corbett, A. H., and Moberg, K. H. ,  
787 2021 The Disease-Associated Proteins Drosophila Nab2 and Ataxin-2 Interact with Shared  
788 RNAs and Coregulate Neuronal Morphology. *In press Genetics*
- 789 Schieweck, R., J. Ninkovic and M. A. Kiebler, 2021 RNA-binding proteins balance brain function in  
790 health and disease. *Physiol Rev* 101: 1309-1370. doi:10.1152/physrev.00047.2019
- 791 Schmitt, A. M., J. Shi, A. M. Wolf, C. C. Lu, L. A. King *et al.*, 2006 Wnt-Ryk signalling mediates  
792 medial-lateral retinotectal topographic mapping. *Nature* 439: 31-37. doi:10.1038/nature04334
- 793 Seyfried, N. T., E. B. Dammer, V. Swarup, D. Nandakumar, D. M. Duong *et al.*, 2017 A Multi-network  
794 Approach Identifies Protein-Specific Co-expression in Asymptomatic and Symptomatic  
795 Alzheimer's Disease. *Cell Syst* 4: 60-72 e64. doi:10.1016/j.cels.2016.11.006
- 796 Shafer, B., K. Onishi, C. Lo, G. Colakoglu and Y. Zou, 2011 Vangl2 promotes Wnt/planar cell polarity-  
797 like signaling by antagonizing Dvl1-mediated feedback inhibition in growth cone guidance. *Dev*  
798 *Cell* 20: 177-191. doi:10.1016/j.devcel.2011.01.002
- 799 Shimizu, K., M. Sato and T. Tabata, 2011 The Wnt5/planar cell polarity pathway regulates axonal  
800 development of the Drosophila mushroom body neuron. *J Neurosci* 31: 4944-4954.  
801 doi:10.1523/JNEUROSCI.0154-11.2011

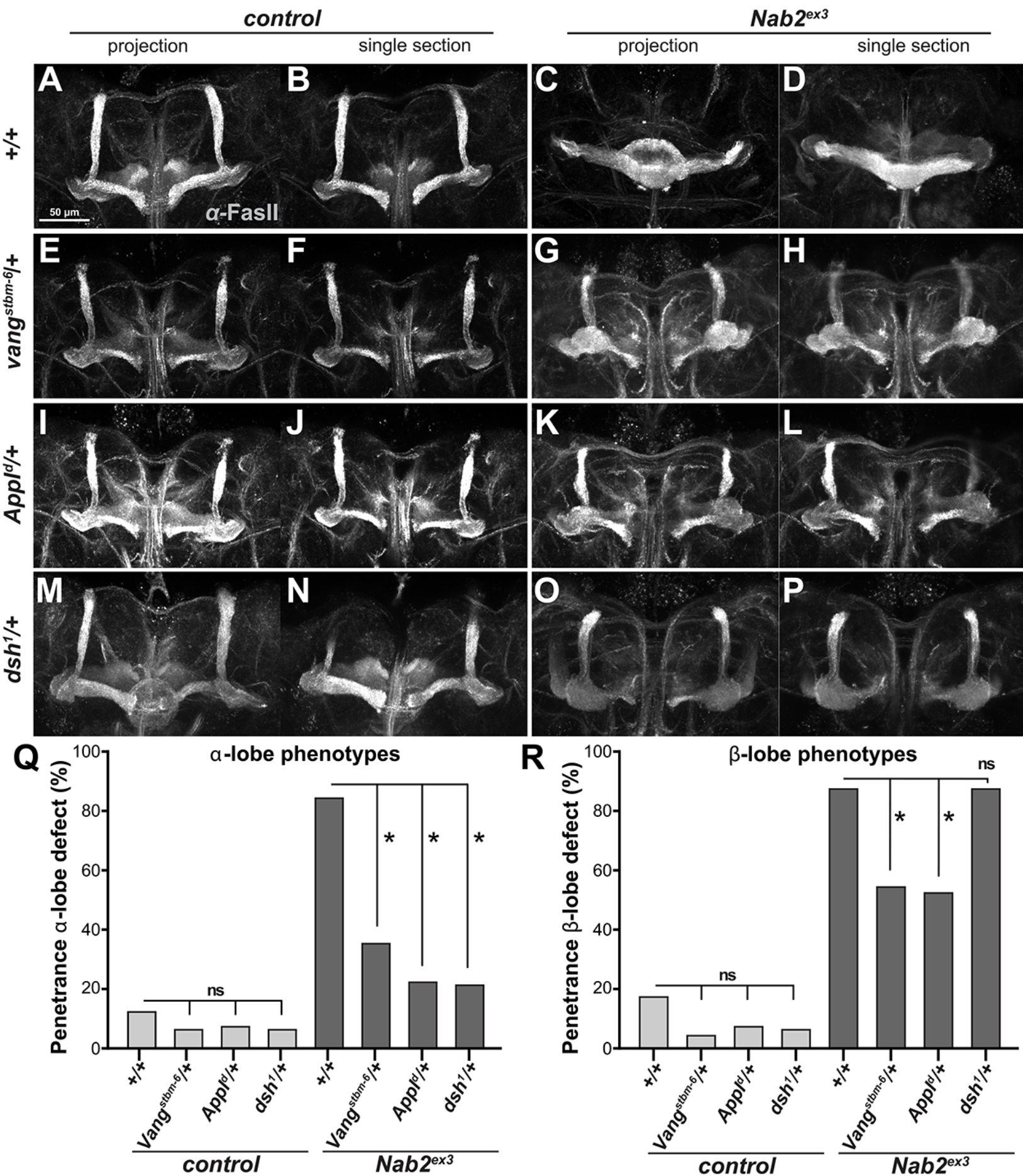
- 802 Simons, M., and M. Mlodzik, 2008 Planar cell polarity signaling: from fly development to human  
803 disease. *Annu Rev Genet* 42: 517-540. doi:10.1146/annurev.genet.42.110807.091432
- 804 Singh, J., and M. Mlodzik, 2012 Hibris, a Drosophila nephrin homolog, is required for presenilin-  
805 mediated Notch and APP-like cleavages. *Dev Cell* 23: 82-96. doi:10.1016/j.devcel.2012.04.021
- 806 Soldano, A., Z. Okray, P. Janovska, K. Tmejova, E. Reynaud *et al.*, 2013 The Drosophila homologue of  
807 the amyloid precursor protein is a conserved modulator of Wnt PCP signaling. *PLoS Biol* 11:  
808 e1001562. doi:10.1371/journal.pbio.1001562
- 809 Sotillos, S., and S. Campuzano, 2000 DRacGAP, a novel Drosophila gene, inhibits EGFR/Ras signalling  
810 in the developing imaginal wing disc. *Development* 127: 5427-5438
- 811 Stoeckli, E. T., 2018 Understanding axon guidance: are we nearly there yet? *Development* 145.  
812 doi:10.1242/dev.151415
- 813 Strutt, H., J. Gamage and D. Strutt, 2016 Robust Asymmetric Localization of Planar Polarity Proteins Is  
814 Associated with Organization into Signalosome-like Domains of Variable Stoichiometry. *Cell*  
815 *Rep* 17: 2660-2671. doi:10.1016/j.celrep.2016.11.021
- 816 Tai, C. Y., A. L. Chin and A. S. Chiang, 2021 Comprehensive map of visual projection neurons for  
817 processing ultraviolet information in the Drosophila brain. *J Comp Neurol* 529: 1988-2013.  
818 doi:10.1002/cne.25068
- 819 Taylor, J., N. Abramova, J. Charlton and P. N. Adler, 1998 Van Gogh: a new Drosophila tissue polarity  
820 gene. *Genetics* 150: 199-210. doi:10.1093/genetics/150.1.199
- 821 Theisen, H., J. Purcell, M. Bennett, D. Kansagara, A. Syed *et al.*, 1994 dishevelled is required during  
822 wingless signaling to establish both cell polarity and cell identity. *Development* 120: 347-360
- 823 Thelen, M. P., and M. J. Kye, 2019 The Role of RNA Binding Proteins for Local mRNA Translation:  
824 Implications in Neurological Disorders. *Front Mol Biosci* 6: 161. doi:10.3389/fmolb.2019.00161
- 825 Thum, A. S., and B. Gerber, 2019 Connectomics and function of a memory network: the mushroom  
826 body of larval Drosophila. *Curr Opin Neurobiol* 54: 146-154. doi:10.1016/j.conb.2018.10.007
- 827 Vldar, E. K., D. Antic and J. D. Axelrod, 2009 Planar cell polarity signaling: the developing cell's  
828 compass. *Cold Spring Harb Perspect Biol* 1: a002964. doi:10.1101/cshperspect.a002964
- 829 Wagh, D. A., T. M. Rasse, E. Asan, A. Hofbauer, I. Schwenkert *et al.*, 2006 Bruchpilot, a protein with  
830 homology to ELKS/CAST, is required for structural integrity and function of synaptic active  
831 zones in Drosophila. *Neuron* 49: 833-844. doi:10.1016/j.neuron.2006.02.008
- 832 Walter, W., F. Sanchez-Cabo and M. Ricote, 2015 GOplot: an R package for visually combining  
833 expression data with functional analysis. *Bioinformatics* 31: 2912-2914.  
834 doi:10.1093/bioinformatics/btv300
- 835 Wang, J., S. Mark, X. Zhang, D. Qian, S. J. Yoo *et al.*, 2005 Regulation of polarized extension and  
836 planar cell polarity in the cochlea by the vertebrate PCP pathway. *Nat Genet* 37: 980-985.  
837 doi:10.1038/ng1622
- 838 Wang, M., P. Marco, V. Capra and Z. Kibar, 2019 Update on the Role of the Non-Canonical Wnt/Planar  
839 Cell Polarity Pathway in Neural Tube Defects. *Cells* 8. doi:10.3390/cells8101198
- 840 Weber, U., W. J. Gault, P. Olguin, E. Serysheva and M. Mlodzik, 2012 Novel regulators of planar cell  
841 polarity: a genetic analysis in Drosophila. *Genetics* 191: 145-162.  
842 doi:10.1534/genetics.111.137190
- 843 Wolff, T., N. A. Iyer and G. M. Rubin, 2015 Neuroarchitecture and neuroanatomy of the Drosophila  
844 central complex: A GAL4-based dissection of protocerebral bridge neurons and circuits. *J Comp*  
845 *Neurol* 523: 997-1037. doi:10.1002/cne.23705
- 846 Wolff, T., and G. M. Rubin, 2018 Neuroarchitecture of the Drosophila central complex: A catalog of  
847 nodulus and asymmetrical body neurons and a revision of the protocerebral bridge catalog. *J*  
848 *Comp Neurol* 526: 2585-2611. doi:10.1002/cne.24512

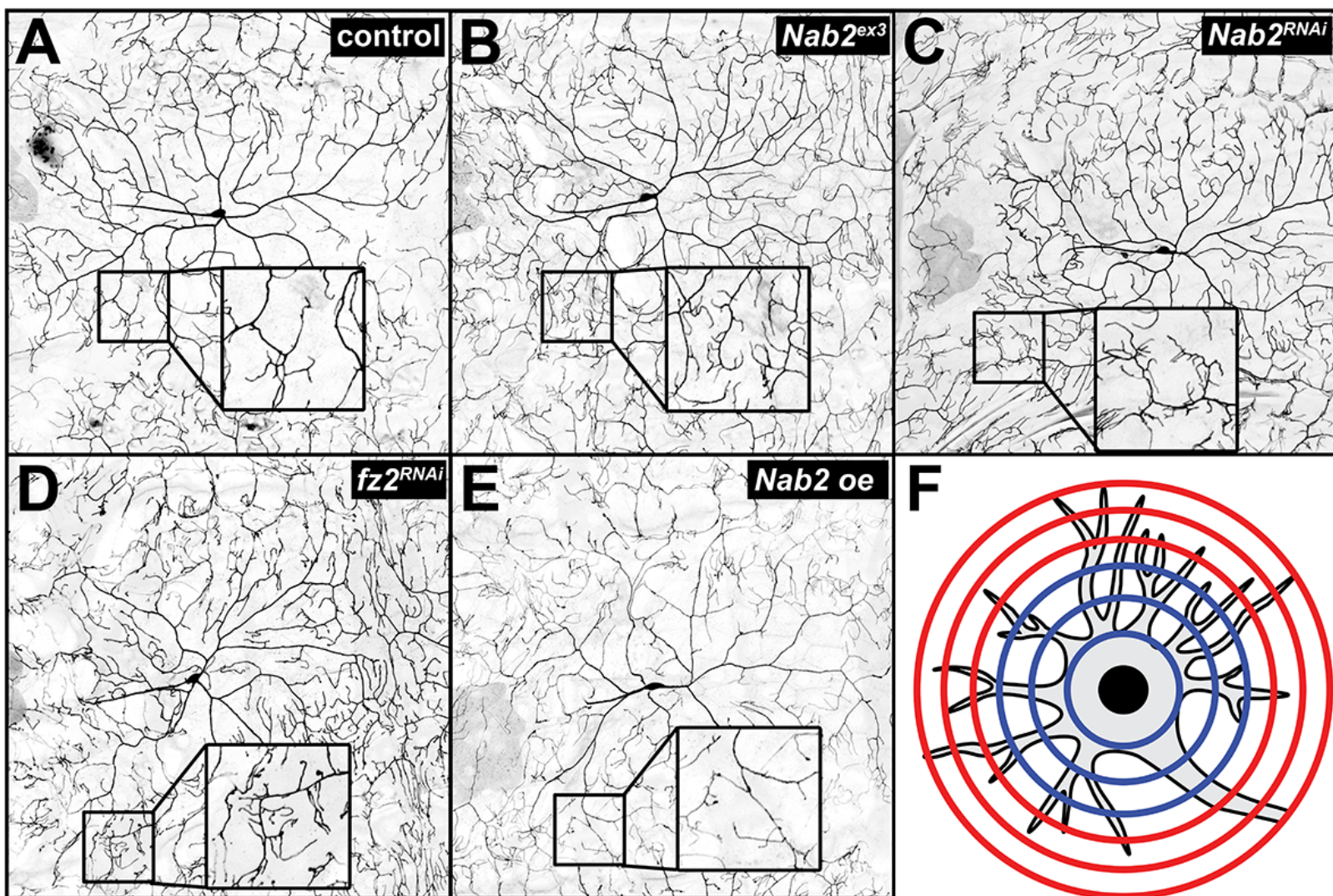
- 849 Yasumura, M., A. Hagiwara, Y. Hida and T. Ohtsuka, 2021 Planar cell polarity protein Vangl2 and its  
850 interacting protein Ap2m1 regulate dendritic branching in cortical neurons. *Genes Cells*.  
851 doi:10.1111/gtc.12899
- 852 Yoshioka, T., A. Hagiwara, Y. Hida and T. Ohtsuka, 2013 Vangl2, the planar cell polarity protein, is  
853 complexed with postsynaptic density protein PSD-95 [corrected]. *FEBS Lett* 587: 1453-1459.  
854 doi:10.1016/j.febslet.2013.03.030
- 855 Zheng, C., M. Diaz-Cuadros and M. Chalfie, 2015 Dishevelled attenuates the repelling activity of Wnt  
856 signaling during neurite outgrowth in *Caenorhabditis elegans*. *Proc Natl Acad Sci U S A* 112:  
857 13243-13248. doi:10.1073/pnas.1518686112
- 858 Zou, Y., 2004 Wnt signaling in axon guidance. *Trends Neurosci* 27: 528-532.  
859 doi:10.1016/j.tins.2004.06.015
- 860 Zou, Y., 2012 Does planar cell polarity signaling steer growth cones? *Curr Top Dev Biol* 101: 141-160.  
861 doi:10.1016/B978-0-12-394592-1.00009-0  
862



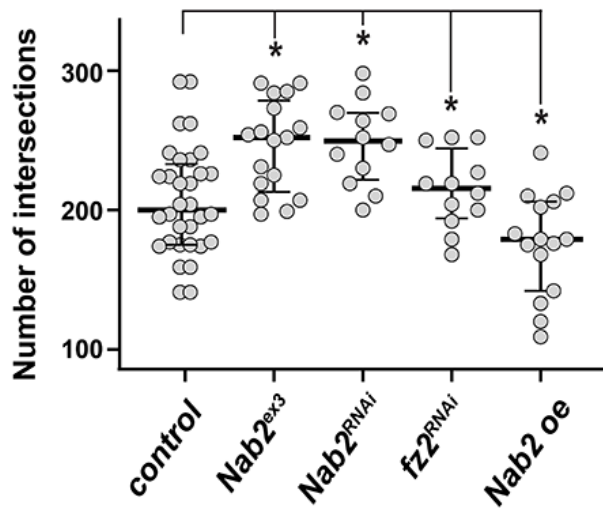
**C**



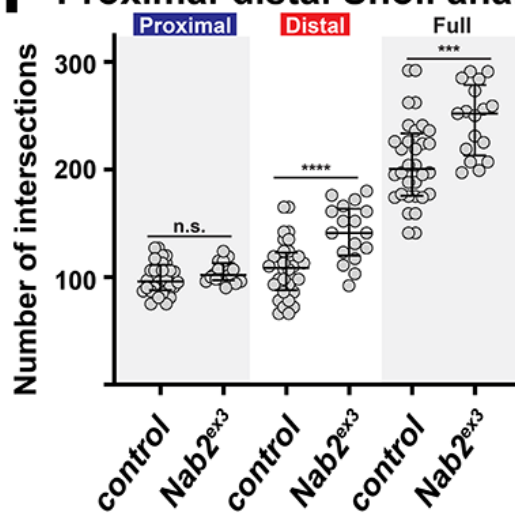


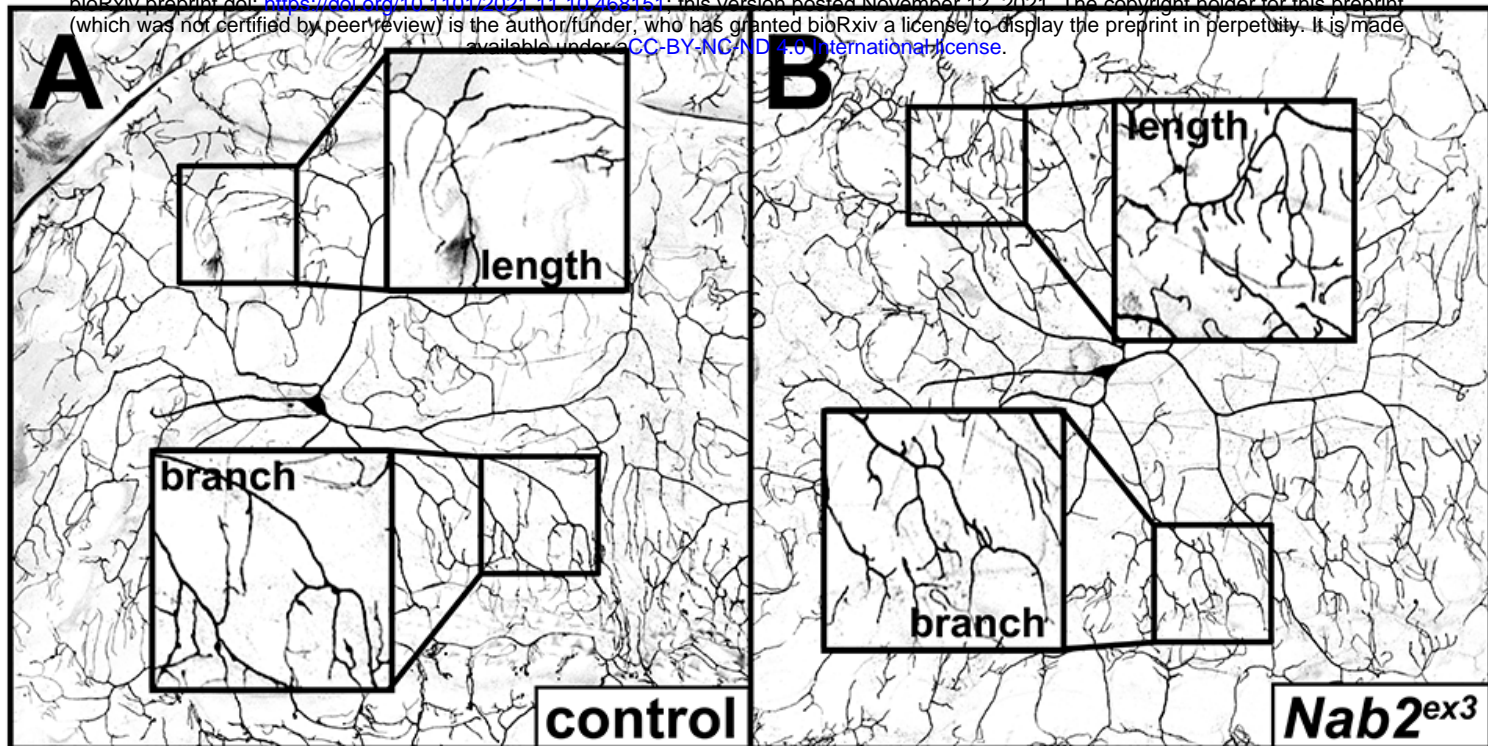


### G Sholl analysis of *ddaC* arbors

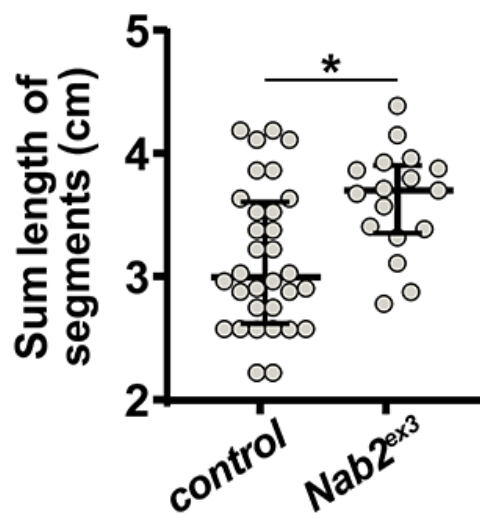


### H Proximal-distal Sholl analysis

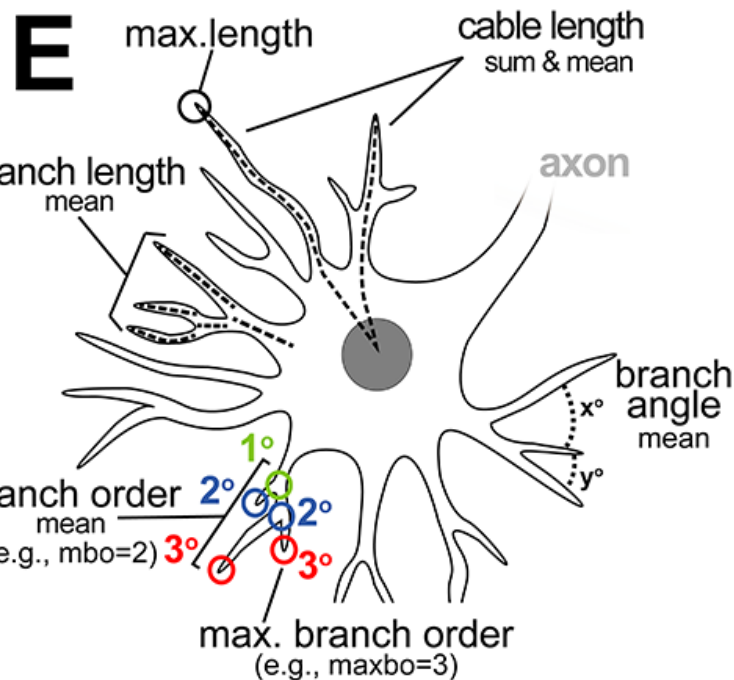
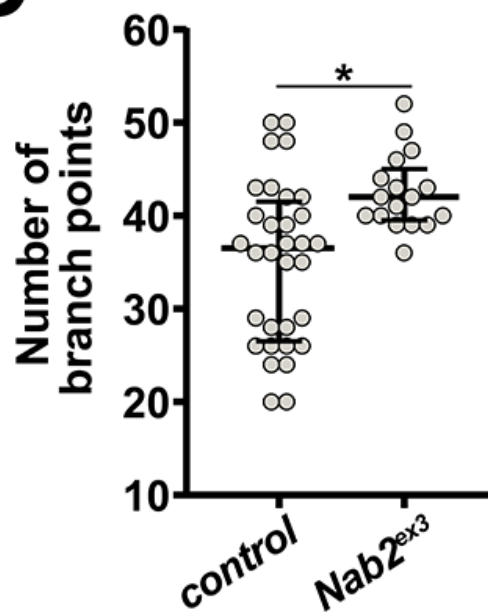




**C** Total cable length



**D** Maximum branch order



**F** *Nab2<sup>ex3</sup>* dendritic phenotypes

